Ultrashort Laser Ablation of Cortical Bone: Literature Review and Experimental Evaluation

Ghadeer W. Khader
McMaster University, khadergw@mcmaster.ca

ULTRASHORT LASER ABLATION OF CORTICAL BONE: LITERATURE REVIEW AND EXPERIMENTAL EVALUATION

By:

GHADEER W. KHADER, B.Sc.

A Thesis

Submitted to the School of Graduate Studies

in Partial Fulfilment of the Requirements

for the Degree

Master of Applied Sciences

McMaster University

MASTER OF APPLIED SCIENCES (2013) McMaster University

(Engineering Physics) Hamilton, ON

TITLE: Ultrashort laser ablation of cortical bone: literature review and experimental evaluation

AUTHOR: Ghadeer W. Khader, B.Sc. (Hashemite University)

SUPERVISOR: Professor Qiyin Fang

NUMBER OF PAGES: xvi, 120

ABSTRACT

Mechanical instruments, such as saw and bur are commonly used for bone cutting during orthopedics surgeries. These conventional instruments showed good bone removal efficiency. Nonetheless, there are some issues with the use of the mechanical tools, such as ill-placed screws and elevation of tissue temperature, which results in thermal damage to the surrounding tissues. These difficulties accompanied with using mechanical tools led to laser ablation investigations.

Lasers, including continues wave (CW) and pulsed, were considered to be a promising tool for bone ablation. When compared to mechanical tools, lasers produce less thermal damage to the surrounding tissues due to their ability to focus on a very small spot, which also produces more precise ablation. Lasers also produce no significant mechanical vibrations within the surrounding tissue and thus less mechanical damage and cracks occur during ablation. Performances of laser ablations are measured by several factors; such as collateral damage, machining time, ablated depth, and ablative precision.

In this thesis work, a literature review was conducted with the aim of understanding the bone characteristics that are related to the optical properties of bone, which leads to a better understanding for ablation mechanisms. This helps in a proper choice of laser parameters for a certain tissue ablation, and thus avoiding collateral damage.

Some laser parameters (pulse energy, scanning speed, and number of passes) were characterized as a first step towards producing large holes. The effect of each one of these laser parameters on the groove depth was found. The feasibility of the ultrafast laser in creating large scale holes was examined, using two scanning strategies: (i) concentric circles scanning, the largest crater depth measured using this procedure was 3.81 mm, (ii) helical scanning, which was used to reduce the machining time, using this procedure a micropillar was created with 12 passes in just 2.5 minutes.

ACKNOWLEDGMENTS

All the praises are due to God who provided me with the ability and intellectual capacity to achieve this progress in my education.

After that, I would like to thank my supervisor Dr. Qiyin Fang for his support, guidance, and motivation in my two years' journey, which was successful because of him. I am thankful for the opportunity he gave me to attend the SPIE conference in San Francisco, where my interest in research grew. Additionally, I am grateful for his patience and overlooking my mistakes, and his kind advice for my future plans.

I would also like to thank Dr. Harold Haugen and his laser lab members Dr. Ran An and Bing Liu for their help and assistance in performing my experiments. I am indebted to Dr. Greg Wohl for his valuable guidance and directions in the biological aspect of my project. I also want to thank Dr. Mark Hurtig and Michele from the Orthopaedic Research Laboratory in Guelph University for their great assistance with Micro-CT imaging.

Special thanks to my dear friends, Meriem Zouari, Aparna Murthy, and Laila Riahi, for their great support and standing by my side when times got hard.

I would like to take this opportunity to express my sincere thanks to the Jordan Education for Women Empowerment and Learning Society (JEWELS) for their generosity in funding. I am greatly indebted to Mrs. Hala Bsaisu Lattouf, Ms. Zahira Haram, Mrs. Zein Shubailat, Mrs. Bassouma Abu Jaber Ghawi, Mrs. Josephine Gammo, Mrs. Azza Hamoudah, Mrs. Tayma Kawar, Mrs. Suad Quteishat, and Mrs. Rasha Qudisat

for their motivation and confidence in me, and for giving me the opportunity to see the world from a different perspective. Additionally, I am thankful to HE Mr. Mark Gwozdecky, the Canadian Ambassador to Jordan, HE Ms. Margaret Huber, HE Ms. John Holmes, and his wife Mrs. Carol Bujeau Holmes, the champion behind JEWELS idea, who helped make this happen.

My acknowledgements would not be complete without mentioning my parents, Wael Khader and Ghada Asaad, my Aunt, Nawal Khader, and my siblings, for their great support and sacrifices to help me follow my dream.

Thank you all from the bottom of my heart…

DEDICATION

To my dad, my real inspiration, who did not live to see this day …

To JEWELS, for their investing in my future …

TABLE OF CONTENTS

LIST OF FIGURES

LIST OF TABLES

LIST OF SYMBOLS AND ABBREVIATIONS

CW – continuous-wave
CPA - chirped pulse-amplifier
μ_a – absorption coefficient
μ_s – scattering coefficient
Nd:YAG – neodymium: yttrium-aluminum-garnet
Er:YAG – erbium: yttrium-aluminum-garnet
Ti:Sapphire – Titanium: Sapphire
Nd:YLF - neodymium: yttrium-lithium-fluoride
Er:YSGG – erbium: yttrium-scandium-gallium-garnet
Ho:YAG- holmium: yttrium-aluminum-garnet
KTP- potassium titanyl-phosphate
Nd:YVO_4- neodymium doped yttrium orthovanadate
PDT – photo-dynamic therapy
T_R – thermal relaxation time
CCD – charged-coupled device
τ – optical delay time
k- tissue thermal diffusivity
δ- optical penetration depth
CT – computed tomography
OCT – optical coherence tomography
SEM – scanning electron microscopy
$w0$ – laser beam waist
ϕ – fluence (J/cm^2)
ξ – incubation coefficient
f – objective lens focal length
AP- alkaline phosphatase
NIR- near infrared
LLLT- low-level laser therapy
ArF- argon fluoride
KrF- krypton fluoride
XeCl- xenon chloride
XeF- xenon fluoride
FWHM- full width half maximum
PBS- pellicle beam-splitter
CCEM- Canadian Centre for Electron Microscopy

DECLARATION

I hereby declare that I am the sole author of this thesis. I certify that any ideas, techniques, or any other material of other people included in my thesis, are fully acknowledged. I have included copyrighted materials and I certify that I have got written permissions from the owners.

This is the true copy of my thesis including final revisions, as approved by my examiners.

Chapter 1: INTRODUCTION

This chapter includes a brief overview of the medical applications in orthopedic surgeries and dentistry where bone cutting is required. It also discusses the complications and limitations of the mechanical tools used in orthopedics, such as accuracy, heat zones produced, and temperature rise in bone tissue during drilling. A brief background about laser ablation was introduced with justification of considering ultrashort laser ablation. Finally, the motivation of my thesis work was provided, in addition to my contribution in this field through a brief description of the thesis outline.

1.1 Overview of medical applications requiring bone cutting or drilling

Drilling a hole in bone is frequently required in many surgical procedures, such as orthopedics, where a cylindrical hole in the bone is produced to be suitable for a screw for fixation purposes. For example, creating holes in plate fixation in condylar fractures (Fig.1 a), posterior pedicle screw fixation for patients who are suffering from spinal fractures or spinal tumors, and anterior rod fixation in spinal stabilization procedures (Fig.1 b) [1, 2].

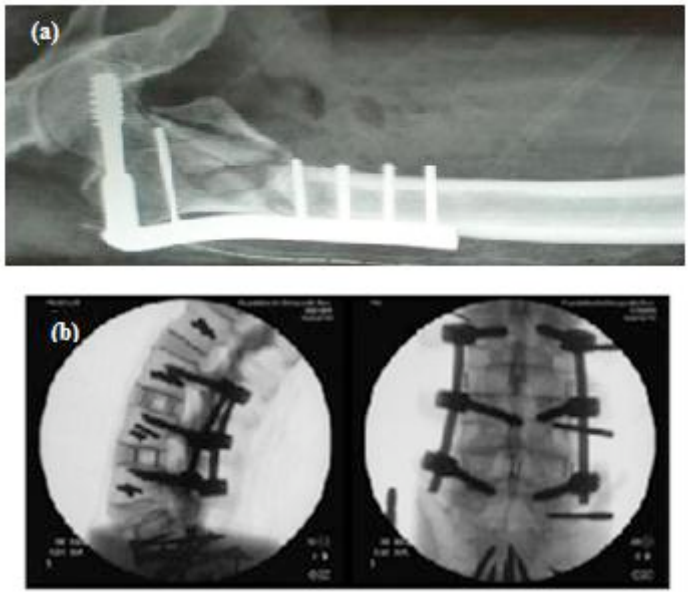

Figure 1: Illustrative examples of typical orthopedic procedures requiring drilling holes on bone: (a) plate is fixed by screws onto a proximal femoral bone for condylar fractures [1]; and (b) spinal stabilization by pedicle screws fixation [2]: lateral (left) and anterior-posterior radiographs (right). Reprinted with permission from [1, 2]

Bone drilling can also be involved in total knee replacement procedures, since some knee implant designs come with pegs, while other implants require screws for further attachment security. In both cases some holes are required to be drilled in the bone tissue during surgery. In dentistry, burr drills are used in dental caries removal and dental implant procedures where an artificial dental root replaces a natural one. A sequence of drilling in the bone layer is performed to create a hole fits the implant as shown in Fig.2 [3].

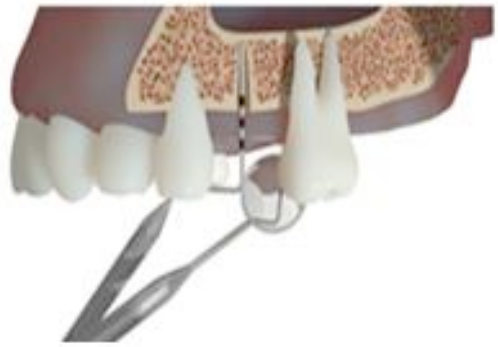

Figure 2: Create a hole in the bone layer in order to insert an implant. Reprinted with permission from [4]

Bone cutting is also required in the removal of bone lesions or tumors, such as osteoid osteomas and osteoblastomas which are common in males in the age between 7-25 years old, and can be found usually in the shaft of long bones (i.e. femur and tibia) [5, 6]. Bone lesions cause pain especially at nights [7], and may lead to bone fracture [8]; so a complete removal for these tumors is required for cure.

1.2 Mechanical tools and their limitations

Procedures that are performed using mechanical burr drills are associated with complications including microfractures in the adjacent bone tissue and heat generation [9]. Mechanized cutting tools usually have high speeds; 10,000- 400,000 rpm in dental applications, and up to 1000 rpm in orthopaedic procedures [9]. This causes a rise in bone temperature that may result in thermal necrosis, which has a negative impact on the bone tissue. Many researchers have attempted to keep the bone temperature below the

threshold that leads to necrosis by reducing the heat generation resulting from drilling [10].

Fig.3 shows an example of heat generation zones that produced during orthogonal cutting. In this case, three regions of heat zones are produced: the energy that accompanies the shearing forces is converted to heat in the region (A) which leads to the plastic deformation zone; shearing forces exist also along the outer face of the tool which leads to the secondary heat region in region (B) however, the heat in this area normally dissipates into the tool, the third heat zone, (C), is generated due to the friction between the tool and the new exposed surface. The maximum temperature within tissue, and thus the thermal damage increases with drill speed [10].

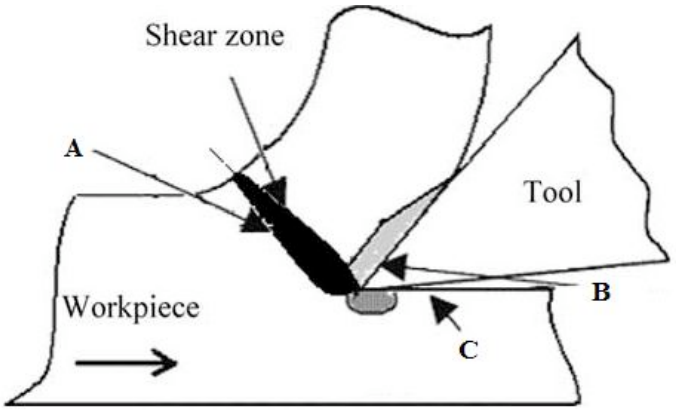

Figure 3: Three heat zones in hard tissue produced by mechanical tool during orthogonal cutting; three heat regions were produced: (A) as a result of shearing forces, (B) secondary heat region produced by the shear forces at the outer face of the tool, and (C) produced by friction. Reprinted with permission from [11]

Osteotomy is an example of such procedures. Oscillating saws and drills were found to cause thermal or/and mechanical trauma to the surrounding tissue due to the mechanical vibrations produced by these instruments which may cause pain and discomfort to the patient, and hemorrhaging in some cases [12]. In addition, these effects can cause cell death and thus delay in the healing process [13].

Mechanical work energy that was produced by mechanical drills is converted into thermal energy deposition in tissue; this can elevate the temperature of the adjacent tissue to a level above the physiological level due to the machining friction and the plastic deformation of tissue [9]. Increase in bone temperature during ablation is a critical factor that affects bone healing and causes tissue damage. This issue is one of the most common problems in dental implant procedures that are performed using mechanical drills since the overheating of bone tissue might lead to bone damage, cells death, and implant failure [10].

Oscillating saw blades that are used in total knee arthroplasty showed temperature elevation of bone up to 100°C. Some studies showed that an increase of bone temperature above 50°C can reduce the regenerative capacity of the bone [9], and a rise in temperature to 56°C-70°C can be harmful for bone tissue, since the transformation of alkaline phosphatase (AP) occurs at this temperature level, which may result in osteonecrosis [14].

Another important issue in mechanical drilling procedures is the ablation accuracy because unnecessary bone removal can affect the screw fixation. Since the bone has non-homogenous and anisotropic properties, in addition to its irregular geometry, it is hard to create holes which are perpendicularly oriented with the bone surface. This will have implications on the final geometry of the cylindrical hole [9].

1.3 Introduction to laser tissue ablation

The unique properties of the laser, such as its high degree of collimation and monochromaticity, give it the ability to produce high intensity pulses in narrow beams. This can produce high-energy light-tissue interactions in a focused area, leading to a precise removal of tissue [15]. Laser ablation is a process in which destruction of material occurs under high-power laser irradiation, followed by removal of a certain volume from its substrate. Lasers have now been used in medical applications for several decades. Lasers were initially considered to be a successful alternative to mechanical tools, due to their ability to focus on a very small spot, and their non-contact ablation [12].

The first laser treatment was reported in 1963 (just three years after the invention of the first functional laser) using a ruby laser, where patients were treated for retinal tears [16]. In the 1980s, studies were carried out to examine the feasibility of using lasers in orthopedic procedures [17-19]. Continuous wave (CW) and long pulsed lasers were used in many of these studies, where the results showed carbonization and fracturing produced in the surrounding tissue [20].

Niemz showed that the ablation process depends on laser irradiance [21]. High laser irradiance can be achieved with low average energy when focused on a small spot area or when the pulse duration of the laser is very short. Picoseconds or shorter pulse durations – commonly referred to as ultrashort pulses – can be achieved by using mode-locked lasers [22]. Ultrashort pulses initiate non-linear interactions with the material which leads to a clean removal process. These pulses also allow the energy to be deposited into material faster than the thermal diffusion rate of the sample, which prevents thermal damage to the surrounding tissue [23].

Thus, ultrashort pulses showed potential in replacing machined tools in orthopedics and dental procedures. My contribution in this field is demonstrated through this thesis. A literature review was conducted in order to present a better understanding of light propagation into bulk, ablation mechanisms and the effect of laser parameters on the ablation process. This may help in the optimization process for laser parameters. The review part was followed by some experiments to test the feasibility of using ultrashort ablation on cortical bone tissue.

1.4 Thesis outline

Chapter 2 of the thesis represents the background. It is a literature review that discusses the histology characteristics of hard tissue in terms of composition and the orientation of the internal structure, which give the bone its unique characteristics. Section 2 of the chapter presents the thermal effect on bone tissue, where the effect of temperature on each bone component was explained. Optimum ablation can be evaluated in terms of the thermal damage results after ablation. The third section of chapter 2 presents the optical properties of bone (i.e. absorption and scattering properties), including the measurement procedure and factors affecting the optical properties.

Section 4 discusses the ablation mechanisms in details, since a good understanding for the ablation mechanism leads to more optimal laser ablation with minimal thermal and mechanical damage. This section differentiates between the various ablation mechanisms, and discusses the laser parameters that can lead to each mechanism. Sections 5 and 6 review several studies that used different lasers in hard tissue ablation. These sections discuss the most common medical applications where each of excimer, CO_2, Er:YAG, Ho:YAG, and Nd:YAG lasers can be used, and the thermal damage zones that each laser produces in hard tissue ablation.

Chapter 3 presents the first part of the experiments, which is the characterization of the ablation parameters, starting with the experimental setup, bone samples, and characterization methods that were used in the experiments. Later, it discusses the effect of several parameters (pulse energy, scanning speed, number of consecutive passes, and pulse duration) on the ablated groove depth. In addition, the ablation threshold measurement methods were discussed, with a brief review for some studies have investigated the factors that affect the threshold. The advantage of ultrashort laser ablation through the incubation effect was illustrated.

Chapter 4 covers the second part of the experiments which is the machining of large size holes. In this chapter two different scanning strategies were discussed: the concentric circles scanning and the helical scanning. Lastly, a summary of the main findings from the thesis work is illustrated in the conclusion part with some suggestions for the future work.

Chapter 2: BACKGROUND

This chapter is a literature review that represents the histological structure of the hard tissue, which is followed by description of the optical properties of bone in terms of scattering and absorption characteristics and the main chromophore at different wavelengths. After that, the ablation mechanisms are discussed in detail, in order to understand the light-tissue interaction process. A brief discussion of medical applications, using different types of lasers, is listed in the end of this chapter.

2.1 Bone histology

Bone cells can be divided into osteoblasts, osteocytes, and osteoclasts. Osteoblasts make and produce new bone by secreting unmineralized organic matrix called osteoid, where the deeper portion of the osteoid undergoes calcification. Some of osteoblasts become enclosed in the matrix to be referred as osteocytes. Osteoclasts act as remodeling cells through resorption of mineralized tissue and break down of bone matrix [24].

Ninety four percent of osteoid is collagen type I that is arranged in triple helix structures made up of two collagen chains, α_1 and α_2, and other non-collagenous proteins. This matrix also consists of inorganic salts such as calcium and phosphate complexes called carbonated hydroxyapatite ($Ca_5 (PO_4)_3OH$) [25], which create platelets with crystal shape in nano meter scale size. The average size of hydroxyapatite crystals is 30 x 3 x 3 nm, and for collagen molecules 300 x 1.5 x 1.5 nm [26]. The combination of osteoid and salts give the bone its hardness and rigidity properties [25]. Connective tissue

in general has a high content of water, and major proteins like collagen or elastin [27]. Calcified bone consists of 20% organic matrix of which 90% is collagen type I, 15- 20% water, 5% carbonates, 1% phosphates, and 50- 60% hydroxyapatite [21, 28].

Basic components in bone structure are (1) the cortical or compact zone, (2) the trabecular zone, (3) periosteal membrane, (4) and endosteal membrane. Due to the rigidity of the cortical zone, it has the ability to resist deformation. The layers in this zone combine tightly together to form osteons and thus have few spaces within it. The trabecular zone is the inner section of the bone which contains the most bone marrow due to its porous nature [24]. The trabeculae of the cancellous bone arranged along the lines of stresses and can be realigned when changing the direction of stress [29]. The periosteal membrane, covering the surface of bones, connects the bone to tendons and muscles. It is made up of innervated and vascular dense fibres. The endosteal membrane forms a thin layer of vascular tissue which lines the marrow cavity. Fig.4 shows the basic components of bone [24]:

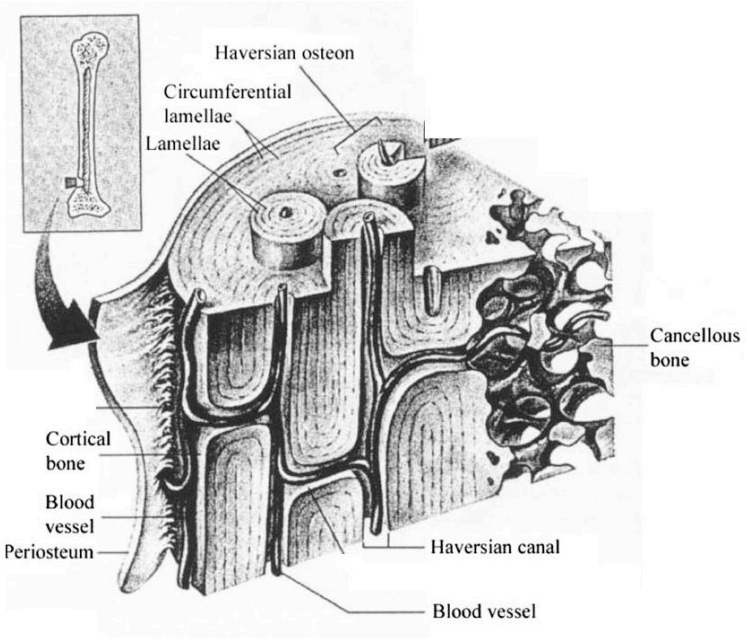

Figure 4: Basic components of bone structure: cortical zone, trabecular zone, periosteal membrane, and endosteal membrane. Reprinted with permission from [30]

In general, bones in the human body are classified into two types depending on the porosity and their microstructure: (1) cortical bone or compact bone and (2) cancellous bone or trabecular bone. Cortical bone, at 5-10% porosity, mostly consists of osteons. It can be found in the shaft of long bones and in the outer shell of spongy bone. Cancellous bone, on the other hand, has a porosity of 50-90% and mostly consists of trabeculae. This type is found at the end of long bones, in flat bones and in the vertebrae [31]. Cortical bone makes up for 80% of the skeletal mass, while trabecular bone makes up the rest, although it has a greater surface area [32].

Fig.5 shows the hierarchical structure of bone in different structure levels: the macrostructure which shows cortical and trabecular bone, the microstructure that consists of osteons and single trabeculae, the sub-microstructure including the lamella, the nanostructure that shows the collagen fiber, and the sub- nanostructure which shows collagen, mineral, and organic proteins [33].

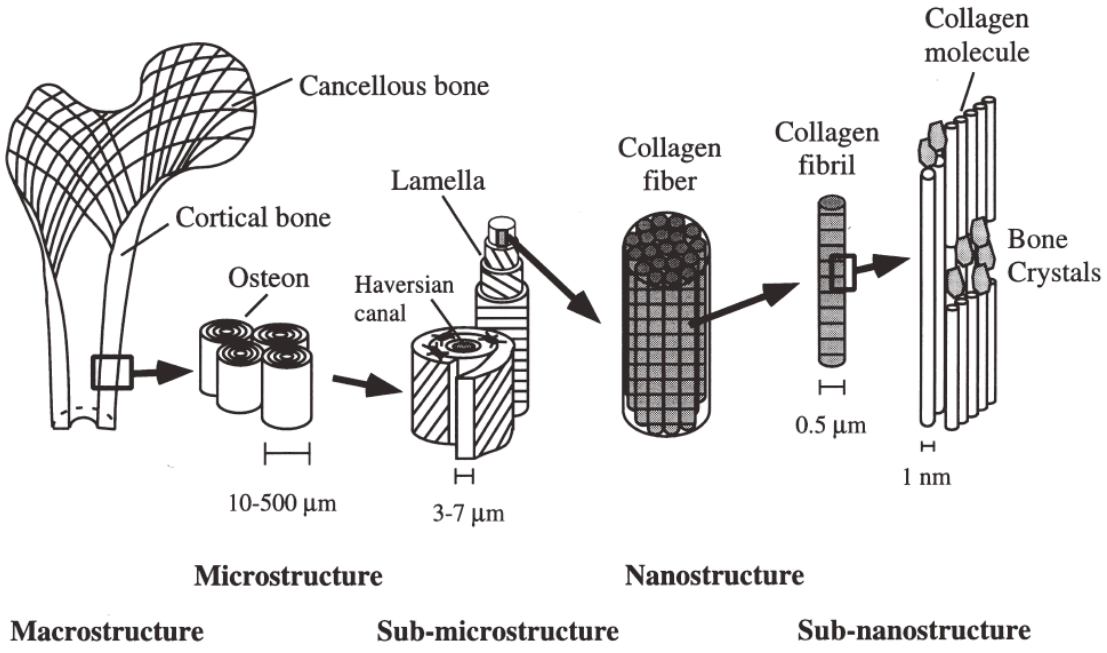

Figure 5: The hierarchical structure of bone in different structure levels: macrostructure, microstructure, sub-microstructure, nanostructure, and sub-nanostructure. Reprinted with permission from [33]

2.1.1 Cortical bone structure

The hierarchical structure divides the bone into three different levels; each level has its own different composition. The first structure level of cortical bone has four different types: woven bone, primary osteon, plexiform bone, and secondary osteon.

The second structure level is made from the components that form osteons: lamellae, osteocyte lacunae, osteocyte canaliculi, and cement lines. Osteocyte lacunae and osteocyte canaliculi are holes in the bone matrix that are involved in cell signaling and host the osteocytes and their processes. The final component, cement lines, is only found in the secondary bone as it results from the remodeling process. This structure level is demonstrated in Fig.6 [34].

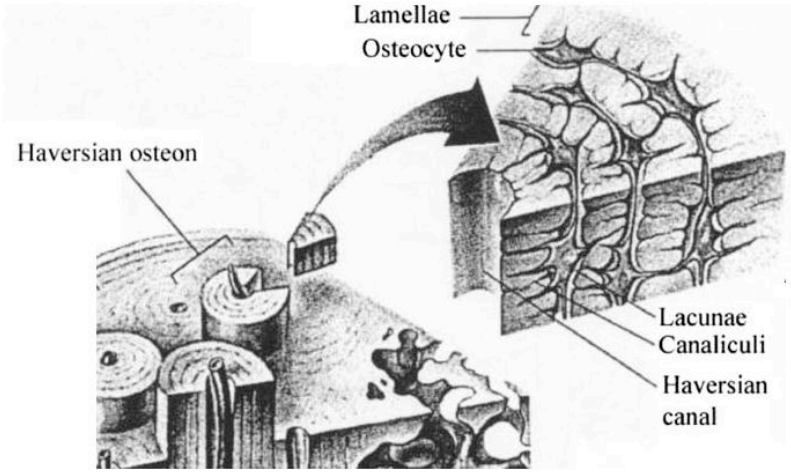

Figure 6: The second structure level of cortical bone that consists from: lamellae, osteocyte lacunae, osteocyte canaliculi, and cement lines. Reprinted with permission from [30]

In the third structure, the cortical bone is divided into two main types, lamellar and woven. Both have collagen fibre type I as their basic component, but they differ in their fibre arrangement. In woven bone, the collagen fibrils are randomly organized unlike in the lamellar bone where it is an organized fashion. This feature is shown in Fig.7 [34].

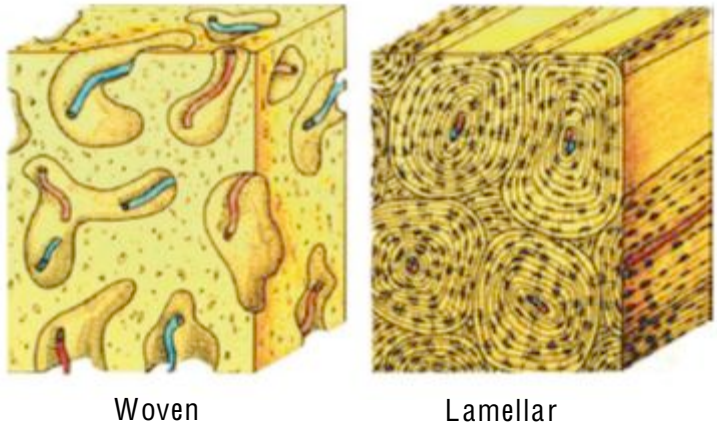

Figure 7: The third structure level of the cortical bone: woven bone (immature bone) that shows randomly arranged cells (osteoblasts and osteocytes) because of the interlacing arrangement of collagen fibers, and lamellar bone (mature bone) where the cells are organized in circular fashion. Reprinted with permission from [34]

2.1.2 Spongy bone structure

At the first level structure of spongy bone, the basic structural entity is the trabeculae. This level does not have blood vessels in it unlike cortical bone. The second and the third levels have the same components as those in the cortical bone [34].

TEM micrographs for cross section of human trabecular bone in Rubin's study (Fig.8) showed that crystals are randomly organized in a circular oriented pattern in certain localized areas. It was found that the orientation of the crystals changes within a 100-200 nm diameter area. The orientation of the crystals depends on the location, as no similar crystal sequences orientations were observed in the nearby regions [35]. In the figure below the black bars indicate the orientation of the crystals:

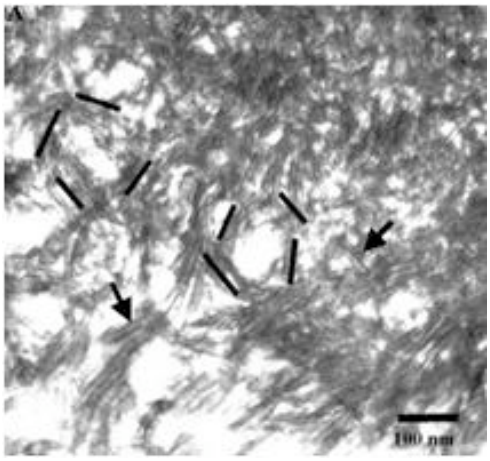

Figure 8: TEM images from Rubin's study shows the circular orientation of crystals in human trabecular bone. Reprinted with permission from [35]

Bone tissue has unique properties which are necessary for living tissue integrity such as high mechanical strength (~100 MPa), high thermal conductivity, and high melting temperature of minerals (~1000 °C). Unfortunately, these properties are unfavorable for laser ablation [36].

2.2 Thermal effect on bone tissue

Heating of biological tissues may cause cell death, protein shrinkage and denaturation, and tissue coagulation. This can alter the tissue structure and thus its properties, such as the mechanical response, specific heat, thermal conductivity and diffusivity [37].

The thermal effect on a particular tissue depends on its components, the response of these components to the heat elevation, and temperature level. Water responds to the heat by boiling until evaporation, if the temperature reaches the boiling limit of water. However, moderate temperatures can cause breaking of a small number of sequential hydrogen bonds in collagen. This can result in collagen unfolding that can return to its natural structure under normal temperatures. High temperatures cause irreversible coiled structure for the triple helix, which can be explained by the breaking of longer sequences of hydrogen bonds that are responsible of the stability of the collagen molecule [37]. The thermal denaturation of tissue proteins controls the thermal damage extent in the surrounding tissue, and affects the dynamic of ablation process [38]. Hydroxyapatite exists in shape of crystallites surrounded by amorphous calcium phosphate and embedded in collagen matrix, so it can withstand high temperatures before melting [39], as the melting temperature of the hydroxyapatite is around 1280℃ [40].

In general, temperature elevation of bone during ablation can result in irreversible damage for the organic matrix of bone [41]. Temperature of 47 ℃ or 50 ℃ that lasts for longer than 1 min is capable to reduce the bone formation, impair bone regeneration, and cause bone necrosis [41, 42]. However, the thermal injury of bone tissue is influenced by

its condition, such as the amount of blood supply and whether it is spongy or cortical [43]. It is also affected by the applied temperature and the exposure time [41].

Tissue damage can result in unfavorable outcomes such as pain, inflammation, and delayed tissue healing [44]. Minimizing tissue damage produced by laser is one of the most important steps towards the optimal ablation. Temperature control during ablation is considered the key factor of successful bone surgery and optimal ablation [45]. Since the thermal effect is controlled by the response of bone components to light propagation, it is important to understand the light-tissue interactions at bulk level.

2.3 Optical properties of bone

The light-tissue interactions are governed by optical properties of tissue [46], as these properties characterize light propagation into tissue [47]. A better understanding of the influence of these properties on light propagation may lead to devise proper ablation strategy that improves ablation efficiency and reduces collateral damage. The purpose of this section is to have a general idea about the optical properties of bone, in order to contribute to a further understanding of the ablation mechanisms [48].

The photons that propagate within tissue may be scattered due to a change in their propagation direction, or be absorbed by molecules and cause electronic transition. The behavior of these photons depends on the optical properties of ablated tissue which are described by absorption coefficient (μ_a) and scattering (μ_s) coefficient. Knowing the optical properties of tissue before starting the ablation may help in determining the

wavelength required, and thus reduce the thermal damage and increase the ablation efficiency [49].

These optical coefficients can be obtained by the following procedure: the diffuse reflection and transmission coefficients are measured (experimentally) using integrating sphere that has light source and detector for optical power measurement. As shown in Fig.9 [50].

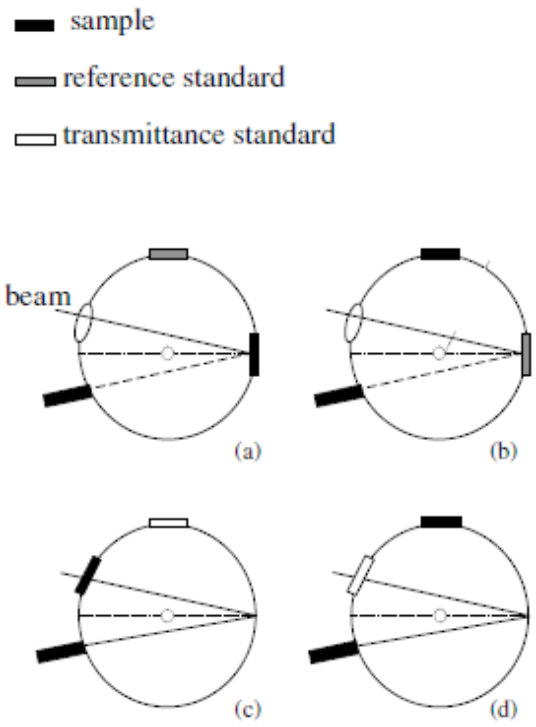

Figure 9: Experimental procedure to measure the reflectance and transmittance of the sample (a and c) and the reference standard (b and d) by using integrating sphere. Reprinted with permission from [50]

Using computer program analysis, such as inverse-adding doubling algorithm or a Monte Carlo algorithm, the theoretical (expected) diffuse reflection and transmission can be calculated at different values of absorption and scattering coefficients. Finally, the experimental measurements of diffuse reflection and transmission with the theoretical values are compared to find the closest match, which yields the absorption and scattering coefficients [50].

2.3.1 Absorption properties of bone

When laser irradiation interacts with biological tissue, the laser energy is converted into heat by absorption. Effective laser ablation is based on the absorption of the target material for laser light. The amount absorbed depends on the absorption properties of the material, characterized by the absorption coefficient. For hard tissue, the dominant chromophore or the main absorber for laser irradiation can be one of the main components of bone (i.e. water, collagen, or minerals), depending on the wavelength of the laser.

Water absorption is the most important factor that contributes to the conversion of laser energy into heat. In addition, most of biological tissues are 60- 80% water. Therefore the absorption of water has the greatest influence on the penetration depth of laser into tissue [51]. At the NIR region, water contributes to absorption starting from 900 nm. The absorption starts weak but rises rapidly with the wavelength to a maximum at 2.94 μm wavelength. The absorption coefficient here is 12000 cm^{-1}. Many studies investigated water absorption at different wavelengths for high water content tissues such

as aorta and skin. It was found that water dominates the NIR absorption spectrum (radiation longer than 1300 nm) [52].

The absorption of water rises with the wavelength in the far infrared region (6- 15 μm). It shows a maximum at 6.1 μm where the absorption coefficient is 2740 cm^{-1}. The optical absorption is considered to be strong when the absorption coefficient is >500 cm^{-1}. In the ultraviolet region (180- 400 nm), water has negligible absorption, but it has a significant absorption level at wavelength of ≤170 nm. Proteins and melanin, on the other hand, are the dominant absorbers at this wavelength region [38]. In general, lasers of near 2 μm wavelengths, such as Ho:YAG laser (2.12 μm), Tm:YAG laser (2 μm), Er:YAG laser (2.49 μm), and Er,Cr:YSGG laser (2.78 μm) have good absorption in water. CO_2 laser also has wavelengths strongly absorbed by water [53]. Lasers that have good absorption are normally absorbed superficially. In general, water has good absorption at Er:YAG laser radiation and CO_2 laser wavelengths [51].

Collagen and water have an absorption peak at 6.1 μm, but the absorption of collagen is more than a factor of 2 higher than the absorption of water at this wavelength. Collagen has another absorption peak at 6.45 μm [38].

Payne showed in his study that at 10.6 μm the absorption of water is dominant, while at 9.5 μm the absorption of collagen and water are equal [54]. In collagen-based tissues, the absorption coefficient drops with the wavelength in the ultraviolet region. For example the absorption at 240- 290 nm wavelengths is 100 times lower than the absorption of this tissue at 190 nm wavelength [38]. Hydroxyapatite has an absorption

coefficient ranging from 3500- 5500 cm^{-1} at CO_2 laser wavelengths, which is 4-9 times higher than those for water at the same wavelengths [40].

The table below lists the absorbance of individual bone component at erbium laser radiation and different wavelengths of CO_2 laser (9.3, 9.6, 10.3, and 10.6 μm) [39].

Table 1: Absorption coefficient of cortical bone components (water, collagen, and minerals) at different wavelengths (Er:YAG wavelength and CO_2 wavelengths) [37]

Bone components	Relative abundance	Absorbance in the individual pure bone components (cm^{-1})					
		Wavelength	2.94	9.3	9.6	10.3	10.6
Collagen	27%		1330	502	556	212	222
Water	13%		11850	554	577	709	817
Minerals	60%		648	5200	5494	4572	3475

From the table we can see that erbium laser (2.94 μm) radiation is absorbed mainly by water component of bone, whereas CO_2 lasers radiation are absorbed strongly by minerals of bone. The absorption coefficient of bone tissue at a certain wavelength depends on the absorption coefficient of each bone component at specific wavelength considering the main chromophore, and the percentage of each component in the bone composition. The following equation is used for bone absorption coefficient estimation:

$$\mu_a = \rho \left(\mu_{HA} X_{HA} / \rho HA + \mu_{H2O} X_{H2O} / \rho H2O + \mu_{Coll} X_{Coll} / \rho_{Coll}\right) \quad (1)$$

Where ρ is mass density and X is weight proportion for each of hydroxyapatite, water, and collagen [55].

To achieve an efficient ablation with minimal thermal damage in bone tissue, the laser penetration should be as small as possible, which means the wavelength of laser irradiation should be chosen such that the maximum absorption of the irradiation occurs within tissue. High laser absorbance leads to highly localized energy deposition within very thin layer [55]. Thermal confinement in this layer reduces the thermal damage and results in precise ablation [56].

Barton found the absorption coefficient of bovine femur cortical bone, which was 5 cm^{-1}, at Ho:YAG irradiation (2.12 μm), considering the absorption coefficient of water (30 cm^{-1} at Ho:YAG wavelength). While in the case of CO_2 and Er:YAG irradiations, the absorption of collagen and hydroxyapatite should also be considered, since they have a significant absorption at these wavelengths. At wavelengths of 2.94 μm and 106 μm, the absorption coefficients of cortical bone have been calculated to be 2413 cm^{-1} and 1803 cm^{-1} respectively [57]. These results show that the absorption coefficient of cortical bone at Ho:YAG radiation was much less when compared to CO_2 (10.6 μm) which was 1803 cm^{-1} and Er:YAG which has the highest absorption (2413 cm^{-1}).

Forrer revealed that although the main chromophore at CO_2 wavelengths is the mineral, water may act as a driving force in bone ablation. This happens when the material destruction occurs by the explosive evaporation of water at certain ablation energy [39]. This claim agrees with B. Payne's results, who investigated the effect of chromophores on the ablation mechanism using CO_2 laser with 9.5 μm and 10.6 μm wavelengths, 180 ns pulse duration and 1 Hz frequency for porcine dermis ablation. In

this study, it was hypothesized before the experiments that 9.5 μm wavelength will result in surface vaporization since the structural matrix is targeted (the chromophore is collagen). But it was observed that the ablation process was driven by an explosive vaporization for both wavelengths, which indicates that tissue chromophores have little or no effect on the ablation mechanism [54].

2.3.2 Scattering properties of bone

Scattering is one of the significant laser-tissue interactions. It is considered the primary step for light-tissue interaction, since it is followed by absorption then heat transition. The photon changes its incident direction when it strikes scattering particles, after that it may transfer some of its incident energy if the scattering was inelastic [58]. Connective tissue has strong inelastic scattering characteristics [27], which may result in undesirable random redistribution in the laser energy [58].

The degree of the optical properties depends on the light propagation direction, which is affected by the orientation of the material components. The internal structure of bone has oriented nature, see Fig.10, which causes multiple scattering of light in the bulk. Reduced scattering is normally used to express the anisotropy property of biological tissue that affects the scattering coefficient. Reduced scattering can be calculated from the following equation [59]:

$$\mu'_s = \mu_s (1 - g) \tag{2}$$

Where μ'_s is the reduced scattering and g is the anisotropy factor. The average g value is 0.93, varying by a few per cent over the wavelength range [59].

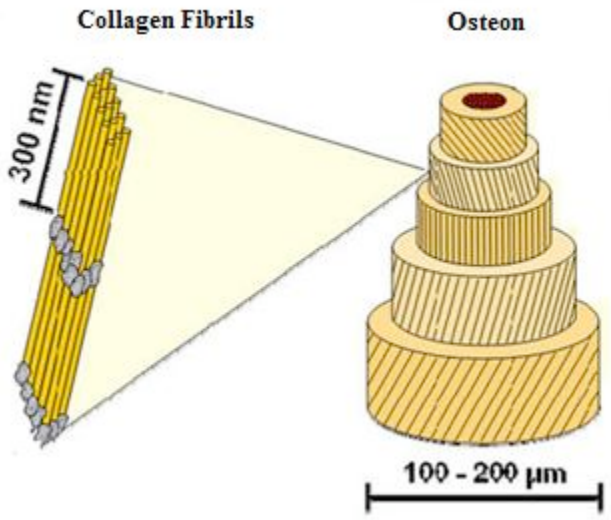

Figure 10: The oriented structure of the cortical bone and the different directions of the collagen. Reprinted with permission from [60]

The optical properties of bone vary from one animal to another. Firbank showed that the scattering coefficient for pig skull bone varies from 35 mm^{-1} to 24 mm^{-1} at 650-950 nm wavelength range, which is much greater than the scattering coefficient of the human skull (2.7- 1.3 mm^{-1}) at the same range of wavelengths [59]. The difference in optical properties of bone among the animals can be related to the difference in relative contents of the main components in each animal bone. Ugryumova et al. showed the effect of mineral content in a porcine skull bone on its optical properties. The samples were immersed in formic acid solution for different time periods to reduce the mineral content of bone gradually. It was found that demineralized samples have lower absorption and

scattering coefficients when compared to the mineralized samples, as shown in Fig.11 [50].

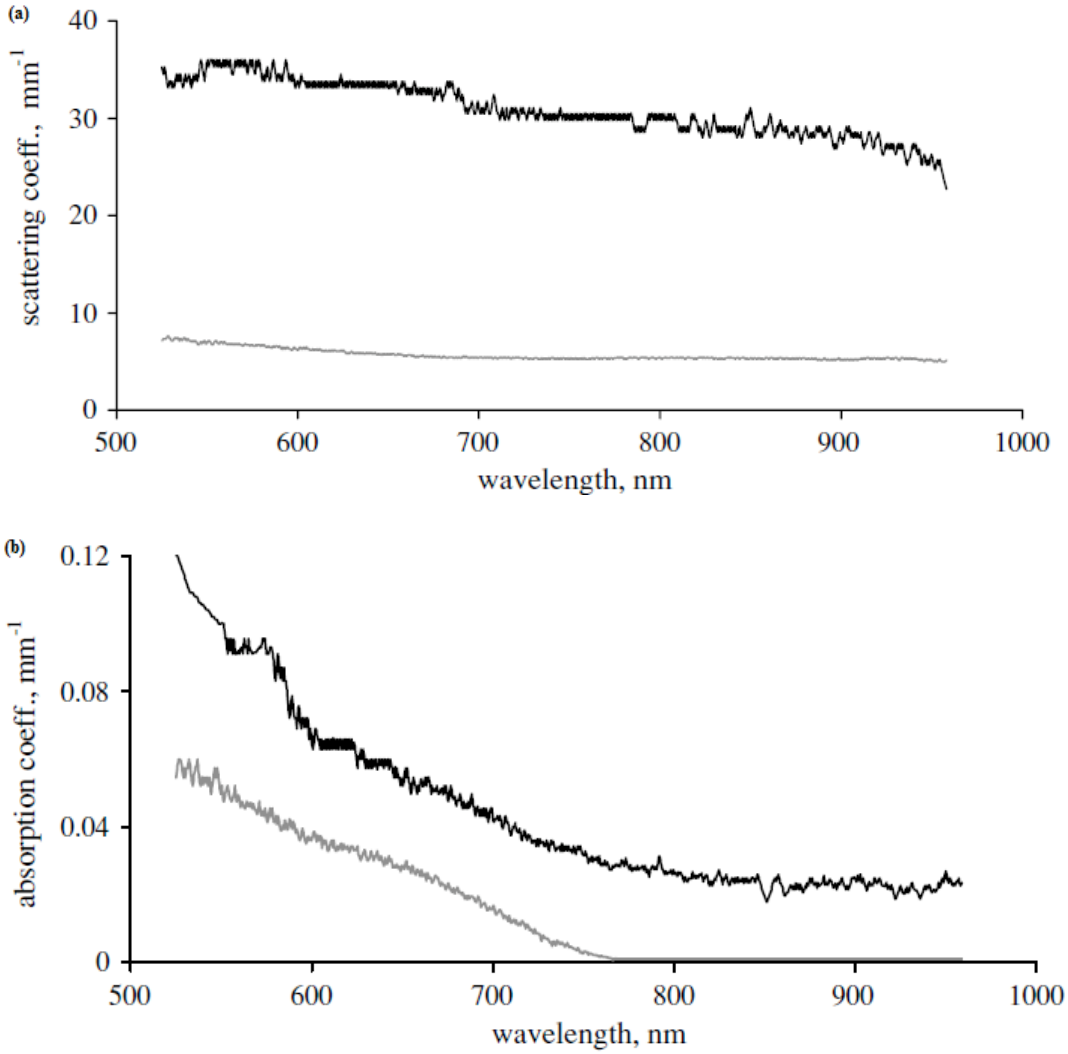

Figure 11: Scattering coefficient (a) and absorption coefficient; (b) of porcine skull as function of wavelength for samples before and after demineralization; where the black lines show samples before demineralization, and grey lines show samples after demineralization. Reprinted with permission from [50]

Bone optical properties depend also on the wavelength. Rossi et al. investigated the dependence of μ'_s and μ_a on the wavelength for porcine femur bone. The results showed that μ'_s has an inverse relation with the wavelength. Since the lower scattering results in higher ablation efficiency, then the wavelength of the laser and its effect on the scattering coefficient should be considered [61]. In general, hard tissue has almost negligible scattering characteristics at mid infrared wavelengths. However, at visible and near infrared wavelengths, the scattering should be considered [55]. The thickness of the samples should also be considered. Thinner specimens reduce the probability of multiple scattering of photons within the specimen, where there is an inverse relation between the specimen thickness and the anisotropy factor [48].

The optical properties of ablated tissue can be changed during the ablation process. For example, increasing in tissue temperature has a significant effect on tissue absorption and scattering. A study showed that the absorption coefficient of water for holmium and thulium laser radiation decreased by one third at 100℃ when compared to the absorption coefficient at room temperature. This study suggests that the effect of temperature on tissue absorption cannot be neglected [62].

The combined effect of the optical properties of tissue makes it possible to track the transportation of light. This simplifies the understanding of ablation mechanisms that are mainly dependent on the optical properties of the materials [63].

2.4 Ablation mechanisms

For optimal ablation results, the laser parameters (wavelength, pulse duration, and repetition rate) should be selected in a proper way for certain tissue ablation. For this purpose, an exact description for ablation mechanisms should be understood.

The material should undergo some changes of its solid phase such as transformation to gas or plasma, for ablation to occur. The phase transformation process depends on the incident laser parameters such as wavelength and pulse duration. Depending on the chosen parameters, and thus the phase transformation mechanism, different ablation mechanisms can occur. The laser-tissue interaction processes can be divided into five main mechanisms depending on the power density of the laser and the exposure time. Fig.12 summarizes these ablation mechanisms.

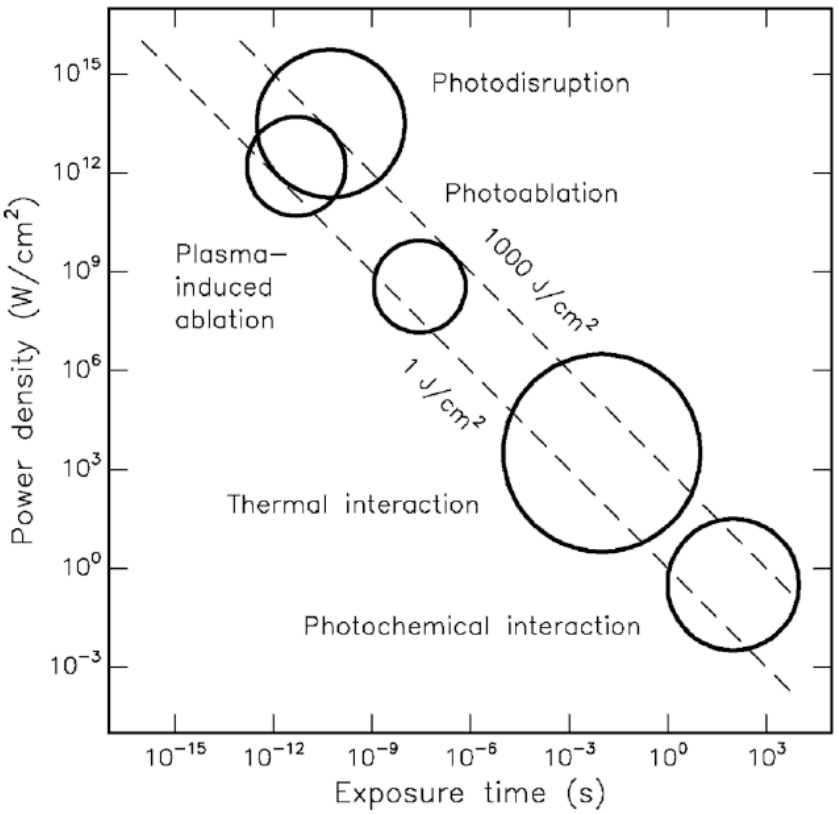

Figure 12: Map of five laser-tissue interaction regions; each mechanism was represented in a circle showing the power density versus the exposure time at which each mechanism can occur. In the energy density range 1 J/cm^2-1000 J/cm^2 (the dotted lines area), all five mechanisms can occur. Reprinted with permission from [21]

2.4.1 Photochemical mechanism

This ablation mechanism can be initiated by laser beams that are continuous waves or have long pulse durations (~seconds scale) with low power densities (~1 W/cm^2). These induce chemical reactions within the targeted tissue [64]. Lasers that can initiate photochemical interactions are those that have visible wavelengths such as red dye and diode lasers, or ultraviolet wavelengths [64, 65].

These lasers are usually used in photodynamic therapy (PDT) to treat cancers, and in low-level laser therapy (LLLT) such as bio-stimulators in cell proliferation for wound healing and hair growth purposes [64, 65].

2.4.2 Photothermal mechanism

Photothermal ablation is considered a slow thermal process, where the irradiation energy is absorbed by the bulk, and then converted into heat which increases the local temperature of tissue. In this process, the transition of the material solid phase happens stepwise [66]. Several heat effects can result while the temperature increases, until the boiling of tissue liquid occurs. This is followed by vaporization and decomposition of tissue fragments and thus ablation [64]. The most basic requirement for ablation is an input of a sufficient amount of energy into the tissue. In general, biological tissues, which are 70% water, require 2500 J/cm^3 for water vaporization [46, 67].

This requirement can be achieved by long wavelengths such as visible and infrared regions, at which the photons have low energy and are well absorbed by water [68]. Higher absorption for laser wavelength, results in vaporization at lower energy, and thus less energy diffusion to the adjacent tissues [69]. These wavelengths should be delivered continuously or as long pulses (1μs- 1 min). These pulses should be long enough when compared to the equilibrium timescale at which the energy transfer between free electrons (that produced after absorption) and ions reaches to equilibrium [68].

In general, lasers that are used to produce this ablation mechanism are CO_2, Nd:YAG, Er:YAG, Ho:YAG, and diode lasers, with power densities of 10 - 10^6 W/cm^2 [64].

Thermal interactions can result in four different observations in the bone tissue depending on the temperature: coagulation, vaporization, carbonization, and melting [64].

Coagulation of the ablated tissue is produced when the local temperature is raised to be ≥ 60 ℃. Denaturation of collagen and proteins of the tissue and cell necrosis also occurred at this temperature. The coagulated tissue is a darker layer when compared to the surrounding tissues [64].

The absorption of laser energy is controlled by the absorbing chromophore. This chromophore is determined by the chosen wavelength. Regardless of the chromophore, the ablation is driven by an explosive vaporization of water which acts as a reservoir for the thermal energy which results from laser conversion [46].

When the temperature reaches 100 ℃, water starts to boil and then vaporize. This can result in microexplosions if the rate of laser energy deposition within the tissue was faster than the rate of energy consumption by vaporization, which leads the water to undergo superheating. During this process, the vapor pressure drives bubble growth which should overcome the surface tension and the tissue matrix elasticity (bubble growth requires a little of vaporization to occur). The boiling continues until the pressure exceeds the ultimate tensile strength of the extracellular matrix. Due to thermodynamic fluctuations, different sizes of vapor bubbles will be formed and will collapse [70], which eventually results in shock wave propagation within the tissue, and thus ejection of overheated volume [46]. This process is considered as a thermomechanical mechanism since it involves mechanical ruptures [64].The photothermal explosion mechanism model was

proposed by Oraevsky, Esenaliev and Letokhov, where the fragmentation of tissue occurs due to mechanical forces that are induced by vaporization [37].

When temperature goes higher than 100 ℃, the carbonization effect results where blackening in the surrounding tissue and smoke generation are produced. Tissues melt when the temperature increases to several hundred degrees [64]. In addition, as the laser power increases, the material starts to vaporize through thermal dissociation of molecules, which changes the material to a vapor phase. This ablation process requires high laser energy to be deposited in the tissue for vaporization to occur, and that can cause thermal denaturation on the surrounding tissues resulting in collateral damage zones [71].

The photothermal mechanism is used for coagulation of soft tissue during certain procedures, such as retinal vascular disease, used for melting and vaporizing tissues, and in laser-induced interstitial thermotherapy (LITT) [64, 65].

2.4.3 Photoablation mechanism

Direct breaking of molecular bonds occurs as a result of the interaction between pulsed laser energy (absorption of laser photons) and the electronic states of the material that are located above dissociation limits, where these electronic states are excited by laser absorption. This excitation leads to fragmentation of the polymer chains, which results in increased pressure when numerous bond breakages happen that allow the fragments to escape from the ablated region [67]. This mechanism can be achieved by

very short laser wavelengths with high energy photons or power densities (10^7- 10^{10} W/cm^2) and an exposure time or pulse duration of 10- 100 ns [64].

This mechanism can reduce the thermal damage on the surrounding tissue, since the pulse duration used is shorter than the thermal relaxation time of tissues (the time required for the temperature to diffuse over a distance). The thermal relaxation time can be defined by the following formula, it is usually in the range of microseconds-milliseconds [65].

$$T_R=\delta^2 /4k \quad (3)$$

Where T_R is the thermal relaxation time, k is tissue thermal diffusivity, and δ is the optical penetration depth [65].

The photon energy of lasers decreases with the increase of the wavelength. Table 2 shows different types of lasers with different wavelength and their corresponding photon energies.

Table 2: Different lasers with their corresponding photon energies [64]

Laser type	Wavelength (nm)	Photon energy (eV)
ArF	193	6.4
KrF	248	5.0
XeCl	308	4.0
XeF	351	3.5
Diode	800	1.6
Nd:YAG	1064	1.2
Ho:YAG	2120	0.6
Er:YAG	2940	0.4
CO_2	10600	0.1

The dissociation limit energy of the molecules (e.g. C_2, CO) located in the region of 6 eV to 8 eV (table 3), corresponds to the UV wavelengths shorter than 200 nm (see table 2), such as far ultraviolet at a wavelength of 193 nm. This leads to direct molecular bond dissociation. Visible and near UV wavelengths, such as excimer laser with 308 nm wavelength and energy of 4 eV, can also excite the high-energy electronic states by two-step excitation [46, 67].

Table 3: The dissociation energies for different chemical bonds [64]

Type of bond	Dissociation energy (eV)
C=O	7.1
C=C	6.4
O-H	4.8
C-O	3.6
C-C	3.6
C-N	3.0

Photoablation process can lead to explosive expansion of the material which results in material ejection [67]. This ablation mechanism is found to be a very clean ablation. Lasers which can induce photoablation are the excimer lasers such as ArF, KrF, XeCl, and XeF that are used mainly in corneal surgery applications, such as LASIK [64].

2.4.4 Photomechanical (photodisruption) mechanism

Normally, the absorbed laser energy is converted into a rise in temperature within tissue before the phase transition occurs and then this energy is redistributed by thermal diffusion [70]. The photomechanical model postulates that during the rapid constant heating of tissue by short pulses, absorption of laser pulse leads the pressure to buildup within tissue until it exceeds the strength of material. This model assumes that the tensile stress is responsible for material ablation, since the materials are weaker in tension than in compression [72]. It is known that tensile stresses can lead to the formation of microcracks in formation, and once the stresses exceed the material strength, material ejection, and thus ablation [67].

When an intense short pulse is applied, the tissue will be heated to temperatures higher than the critical in a timescale shorter than the thermal relaxation time of the tissue. That leads to a direct transition of solid phase to plasma [66]. Since the heating rate of tissue is faster than the expansion rate, a compression wave (positive thermoelastic stress) propagates away from the deposition region towards the surface. This wave is followed by a negative stress (tensile) towards the bulk when the compressive wave encounters a point where acoustic impedance is mismatched (e.g. tissue-air or water interface region). The tensile wave propagates back towards the bulk if the tensile stress exceeds the critical rupture pressure of tissue, then spallation of the heated layers from the surface occurs. This process is called photospallation, and requires the combination of high absorption, short pulses, and low fluence laser parameters to occur [70, 71].

Another mechanical removal process, called cavitation, happens when tensile stresses are initiated in a liquid environment, where growth and collapse of cavities can cause rupture in the surrounding tissues. Both spallation and cavitation processes play a role in photomechanical ablation mechanism [73].

The energy density required to initiate the ablation by this mechanism is lower than the energy required for liquid vaporization, so tissue can be removed without the need to vaporize it in a process called cold ablation. Golovlyov et al. found that Nd:YAG laser with pulse duration of 15 ns initiates the ablation at energy smaller than the energy required for liquid boiling, whereas Paltauf et al. showed that the material ejection was initiated at 100 °C when Nd:YAG laser with pule duration of 100 μs was used [67]. Unlike the photothermal vaporization mechanism, the photomechanical mechanism does not require every bond in the material to be broken in order for ablation to occur, so it is considered energetically more efficient [74].

In general, lasers that are used to initiate this ablation mechanism are solid state lasers, such as Nd:YLF, Nd: YAG, and Ti:Sapphire, that have pulse durations in the range of 100 ns - 100 fs and power densities of 10^{11}-10^{16} W/cm^2. This ablation process is used in some medical applications such as lens fragmentation and lithotripsy [64].

Many studies regarded photodisruption as a multi-cause mechanical effect starting from the breakdown and plasma formation, which is followed by secondary effects such as shockwave and then cavitation and jet formation if the breakdown occurs in soft tissue or fluids. These multiple effects take place in different time scales, as shown in Fig.13 [21]:

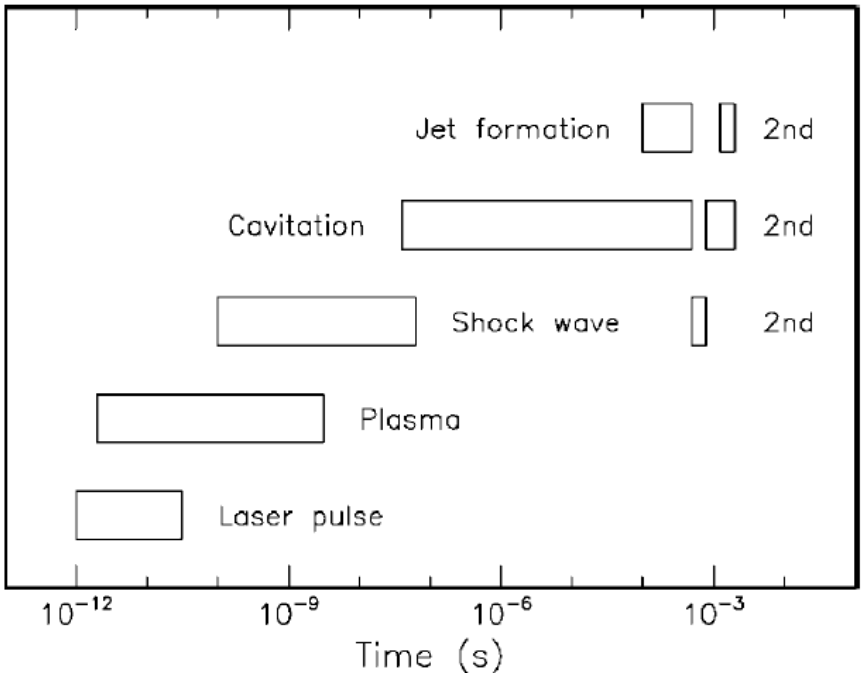

Figure 13: The multiple-effects that cause photodisruption with different time scales. Reprinted with permission from [21]

Plasma formation starts during the pulse and stays for a few nanoseconds to allow the diffusion of free electrons into surrounding material. The plasma expansion causes shockwave generation, after the laser pulse is gone, which is responsible for energy deposition into lattice. This shockwave normally propagates into the adjacent tissue. In soft tissue ablation, the shockwave is followed by a cavitation bubble that is formed 50 -

150 ns after laser pulse, which starts expanding and collapsing. Since the pressure of bubbles increases during collapse, a shock wave will accompany each rebound of bubble, and every collapse can generate a jet formation if it is produced beside a solid boundary [21].

2.4.5 Plasma-mediated ablation mechanism

In general, to remove an atom from solid material the laser intensity should overcome the binding energy for the atom [27, 75]. Pulses with high enough intensity and moderate laser energy can produce high intensities of electric field which can be comparable or exceed the Coulomb potential ($\sim 10^9$ W/cm^2) that binds electrons to ions, then the electrons will experience a force similar in magnitude to the Coulomb force, and thus an excitation of band gap electrons to the excitation band occurs [76], this leads to ionization, and then formation of plasma in the case of plasma-mediated ablation [77].

Plasma-mediated ablation occurs during local excitation through non-linear absorption processes, using pulses that have high instantaneous peaks powers, while keeping low average powers in order to avoid any linear heating for the exposed area [77].

Valence electrons will be ionized by nonlinear ionization mechanisms [76]; such as (a) multiphoton absorption or electron tunneling ionization in which the light directly excites the bound electrons to the conduction band of the material [77], and (b) avalanche ionization where the electrons are already in the conduction band, and they absorb photons to move to higher energy states within the same band. When the energy of the electrons exceeds the conduction band energy, the electrons then start colliding with

molecules until they achieve kinetic energy high enough to ionize other molecules. That will cause further ionization to the material [78], and thus the small-sized plasma will start to expand exponentially. The electrons density keeps growing until the plasma becomes sufficiently conductive to restrict the incident light penetration [77]. It was found that the absorption rates of photons increase in non-linear way with the wavelengths [79].

When all of the electrons become ionized, any other energy absorption will cause a rapid increase in the electron temperature, which means a rapid decrease in light absorbance and increase in light reflectivity in contrast [23]. The ionization process can lead later to the optical breakdown [76].

After the laser pulse ends, the free electrons tend to recombine with the positive ionized molecules in the exposed area in a picoseconds time scale, leading to transfer of the energy from the electrons to the material and results in increasing the internal pressure. This pressure causes rupture in the material structure and forms cavitation bubbles that expand to be associated with shockwave propagation into the surrounding tissue and causes damage [77].

Low-density plasma can be created if an intermediate fluence is applied, which has the ability to produce free electrons. However, the intermediate fluence is insufficient for further ionization of molecules, and thus a high-density plasma may not be created, even though this low- density plasma can result in chemically and thermally modification in the local tissue [77].

Plasma temperature can reach to 15000 °C and even higher which can vaporize the solids, pressure may associate the plasma and results in phase change such as vaporization, melting, and thermal expansion of the tissue. The absorption of the photons by plasma can prevent the transmission of photons to the target. This phenomenon is known as plasma shielding [69].

In general, plasma mediated ablation can be initiated with ultrashort laser pulses in the range of 500 ps to 10 fs with power densities of 10^{11}-10^{13} W/cm^2, which can be produced by some lasers such as Nd:YAG, Nd:YLF, and Ti:Sapphire. This type of ablation mechanism is applied in corneal surgery, dentistry, and diagnosis [64].

Both plasma mediated and photodisruption processes rely on plasma formation and have the same interaction time, so it is a quite difficult to distinguish between these two interactions [21]. However, we may say that the plasma-induced ablation occurs when using nanoseconds laser pulses, however for shorter pulse durations, both plasma-induced ablation and photodisruption may occur [80].

The table below summarizes the ablation mechanisms with regards to laser parameters required to initiate each mechanism, the interaction responsible for the ablation process, and the medical applications for each mechanism.

Table 4: Summary of the ablation mechanisms, shows the laser parameters required to initiate each mechanism, the interaction responsible for the ablation process, and the medical applications for each mechanism

Ablation mechanism	Laser parameters			Laser type	Interaction	Medical applications
	Pulse duration	Power density	Wavelength			
Photo-chemical	Sec - CW	1W/cm^2	UV-visible	Dye and diode	Chemical reactions	-Photodynamic therapy -Cell proliferation
Photo-thermal	1μs-CW	10-10^6 W/cm^2	IR	Nd:YAG Er:YAG Ho:YAG CO_2	Heating until vaporization OR Microexplosion	Coagulation/ melting/ vaporizing of soft tissue
Photo-ablation	10-100ns	10^7-10^{10} W/cm^2	UV	Excimer	Direct dissociation of molecular bonds	Corneal surgery (LASIK)
Photo-disruption	100ns-100fs	10^{11}-10^{16} W/cm^2	NIR	Nd:YAG Ti:Sapph	Tensile stresses	-Lens fragmentation -Lithotripsy
Plasma-mediated	500ps-10fs	10^{11}-10^{13} W/cm^2	NIR	Nd:YAG Ti:Sapph	Plasma expansion	-Corneal surgery -Dentistry

2.5 Applications of lasers in medicine: review

The first medical contribution for laser, in hard tissue ablation, was reported in 1965 where a human tooth ablation was carried out by Goldman et al. using ruby laser [81]. However, the first dedicated laser considered for the dentistry was Nd:YAG (1064 nm) which was developed by Terry Myers in 1989 [81]. Later studies showed that CO_2 and Er:YAG lasers can also be used to cut the bone precisely and with low carbonization or mechanical stress effects [82].

The potential of any laser type for bone ablation can be characterized by measuring the morphological change of tissue after irradiation, ablation rate, ablation threshold, and ablation efficiency. In this section, various types of lasers and their feasibility in hard tissue ablation will be reviewed. The focusing will be on the thermally altered zones produced by lasers; since each laser heats different volume of tissue depending on its wavelength absorbance, and therefore leaves different zones of thermally altered tissue.

2.5.1 Excimer lasers in medicine

Excimer lasers generate different UV wavelengths depending on the nobel gas halides used in their operation [argon fluoride (ArF) 193 nm, krypton fluoride (KrF) 248 nm, xenon chloride (XeCl) 308 nm, xenon fluoride (XeF) 351 nm]. These UV lasers initiate the ablation by photochemical reaction in which a direct bond breaking in tissue molecules occurs due to the high energy photons of the UV irradiation. This process converts the molecules into gaseous plasma [83].

Excimer laser was thought to be a potential instrument for tissue ablation, because of the little thermal effect that results from its radiation [84]. The most common medical application for excimer laser (ArF) is LASIK for vision correction. In orthopaedics, excimer laser showed precise ablation in cartilage, and that was explained by the good absorption of UV irradiation in cartilage tissue. For example, human menisci have maxima absorption at 280 nm and 340 nm wavelengths [83].

The potential of pulsed ultraviolet excimer laser in bone ablation was examined by Sarkar et al., by measuring the ablation rate, ablation threshold, and the damaged zones in bone samples that were taken from pig's skull. The ablation procedure was carried out in vitro using 193 nm, 248 nm, 308 nm, and 351 nm wavelengths, and in vivo by 193 nm wavelength. Nanosecond pulse duration was used (15 ns - 20 ns). They got the highest ablation rate at 248 nm which was 1.4 μm/ pulse, and they found that rate increases sharply with increasing fluence for all wavelengths. They also found that the ablation threshold was increasing with wavelength; the threshold at 193 nm was 335 mJ/cm^2, while it was 16 times higher (~5500 mJ/cm^2) at 350 nm wavelength [69].

The maximum collateral damage in Sarkar's study was measured to be 60 - 75 μm at 351 nm wavelength, which is considered acceptable in the medical procedures, and the minimum thermal damage was obtained at 193 nm which was in the range of 1 - 3 μm [69]. Yow et al. measured a small thermal damage zone of 2 - 3 μm in bone tissue that was treated by excimer laser (308 nm) [85]. Dressel et al. showed that the temperature increase in the surrounding tissue was below 40 degrees during bone ablation by XeCl-excimer laser, which produced carbonization-free samples [84]. Another study of the morphological changes of rabbit tibia bone treated by XeCl-excimer laser (308 nm, 20 ns) where the carbonization and damage of adjacent tissue were not observed [86].

Some studies compared the excimer laser with the mechanical tools in bone ablation, such as König et al. and Walter et al., in which they demonstrated the ability of excimer laser to be used for microsurgery of bones through their experiments on cranial rat bones

that were treated using UV laser with wavelengths of 193 nm and 248 nm. Their studies showed that excimer laser produces no thermal damage, no delay in healing process, and the results were more precise when compared to mechanical tools [87, 88].

Authors demonstrated the feasibility of using excimer laser in bone cutting. It was found that these lasers avoid the bone necrosis and mechanical trauma, and showed high accuracy in bone cut during osteotomy procedures, in addition to their small thermal damage when compared to other lasers such as continuous wave (CW) CO_2 laser [69, 86].

2.5.2 CO_2 lasers in medicine

CO_2 laser is based on gas mixture where the light is amplified by carbon dioxide molecules. Basically, this laser emits wavelength of 10.6 μm, but it can also emit wavelengths in the region of 9-11 μm. CO_2 lasers are widely used in material processing such as cutting and welding metals, plastic, wood, etc. In addition, it contributes to some surgeries such as ophthalmology [89].

Researchers in medical application field have paid attention to the infrared wavelength region, because it has a strong absorption within biological tissue especially at 1.95, 2.94, 6.09 μm, and has a broad absorption at 10 μm. Ablation of hard tissue has been reported in several studies that used different infrared wavelengths of different lasers [39]. CO_2 laser irradiation is strongly absorbed by water, and since most biological tissues have high water content 70-80%, CO_2 irradiation is absorbed in a few tens of microns in the tissue surface [90].

Several tens of Watts of laser power and wavelength strongly absorbed by bone are basic requirements for osteotomy procedures. CO_2 laser meets these criteria; however, it leads to strong charring into tissue, which results in delay of tissue healing [40]. Several studies used CW and long pulses (ms) of CO_2 lasers (9.6 μm and 10.6 μm) for bone ablation. They observed carbonization area in mm scale and necrosis in the ablated samples [36]. That was explained by the ablation mechanism which is followed by CW-CO_2 laser in which the tissue is heated until vaporization and thermal denaturation; thus it has high probability to affect the surrounding area [69].

Studies attempted to reduce the thermal damage resulting from CO_2 laser ablation by using short laser pulses, which leads to fast energy deposition in a small absorption layer (a few μm thick). This results in a strong pressure of evaporated water which can destroy bone structure in temperature much below the melting temperature of the structure, by water explosion mechanism. Other studies tried to reduce the heat generation during ablation by providing sufficient cooling [40, 41]. Water spray during ablation was used as a coolant in several studies in order to reduce the thermal side effects as carbonization, and to produce smooth ablated outlines [91]. For example, Frentzen et al. tested the feasibility of 80 μs CO_2 laser (10.6 μm) with water spray in bone cutting, through studying the collateral thermal damage of pig rib samples after ablation. The laser parameters were chosen in this study (e.g. fast scanning, short pulses) and the use of air/water spray resulted in negligible thermal and mechanical damage, where all the ablated samples were char-free and without cracks, and prevented the accumulation of the heat within tissue [92]. Ivanenko found that using CO_2 laser (9.6 μm) with 300 ns

pulse duration in hard tissue ablation with air-water spray results in charring free ablation of bone and a small thermally altered zone of 2-6 μm, where the air-water spray prevented the heat accumulation during ablation [40].

Fried and co-workers used CO_2 laser (9.3 μm, 400 Hz, 80 J/cm^2) with pulse duration of 5-18 μs, to ablate human dentin and porcine rib bone tissues. They compared the ablation with and without water spray. They found that ablation with water spray produced clean incisions, while ablation without water coolant produced charring in the both tissues. As shown in Fig.14 [93].

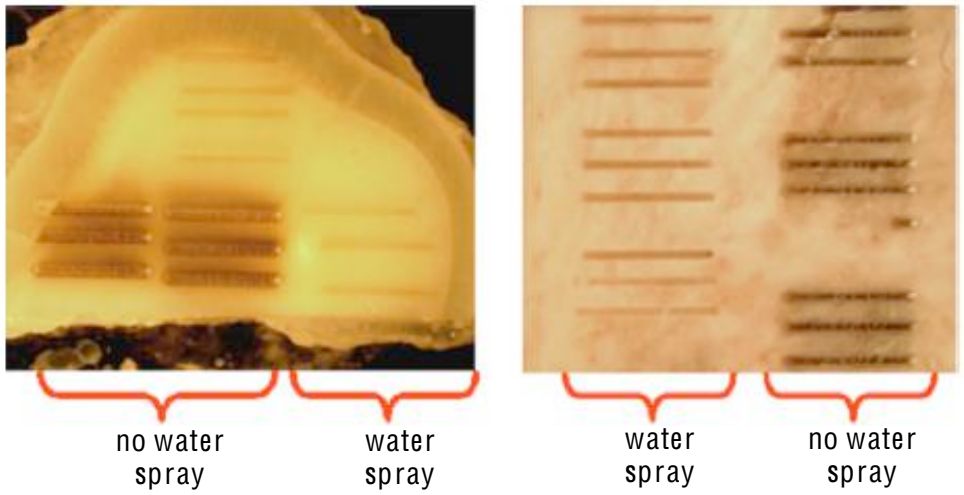

Figure 14: CO2 laser (9.3 μm) ablation for human dentin (left) and porcine rib bone (right) with and without water. Reprinted with permission from [93]

2.5.3 Er:YAG laser in medicine

Erbium-doped: yttrium aluminum garnet (Er:YAG) laser produces 2940 nm wavelength (in the infrared region), which matches the maximum absorption in water, and that is 10-15 times larger than water absorption for CO_2 (10.6 μm) laser radiation [94, 95]. Because of the high absorption in water, Er:YAG showed an effective ablation with low thermal damage in different medical applications, such as periodontics and oral surgeries [96]. Perez and Bank demonstrated that Er:YAG laser can be effective in skin resurfacing, where new collagen formation is induced by laser, and their results showed that the healing period required after Er:YAG treatment is shorter than that required when short pulses of CO_2 laser are used [94]. Furthermore, the ablation threshold for the skin was found to be 1.6 J/cm^2 [97] that is much lower than 5 J/cm^2 which is the threshold when CO_2 laser is used [94].

In case of hard tissue ablation, Er:YAG results in less temperature elevation in the ablated tissue when compared to CO_2 laser ablation, and accordingly smaller zones of thermal damage are produced. That can be referred to the difference in the ablation mechanism for both lasers. CO_2 radiation targets hydroxyapatite where the absorbed energy is converted to heat and increases the tissue temperature to over 700 °C which is high enough to melt the hydroxyapatite, this ablation mechanism is classified as thermal vaporization. In contrast, Er:YAG irradiation is strongly absorbed by water when compared to hydroxyapatite; the ablation mechanism in this case is water micro explosions, which is initiated by water boiling at temperature of 100 °C [98].

B. Gasˇpirc and U. Skaleric investigated the feasibility of Er:YAG laser in dental ablation. The results showed that the physical morphology only was influenced without altering the chemical structure of the proteins. Since the photon energy of Er:YAG irradiation is just 0.42 eV, the probability for breaking the chemical bonds by multiphoton absorption is low [99].

However, studies showed that using water coolant during Er:YAG ablation is effective in thermal damage reduction. Armengol et al. compared the temperature rise in dentin ablated by Er:YAG laser with and without water spray. It was found that the temperature rise without water coolant was in the range of 3.07 ℃- 3.55 ℃ for different dentin thicknesses (2 mm-1 mm) respectively, while the temperature rise with water spray was in the range of 0.75 ℃- 0.96 ℃ for 2 mm-1 mm thicknesses respectively [100].

2.5.4 Ho:YAG laser in medicine

Holmium: yttrium-aluminum-garnet (Ho:YAG) laser is considered the most versatile laser in the medical applications. This laser has wavelength of 2.12 μm which has a good absorption in water, and it has the ability to vaporize, coagulate and ablate soft and hard tissues [101]. Ho:YAG laser is used in different medical applications, such as prostatectomy [102], fragmentation of ureteral stones [103, 104], and bladder tumor treatment [105].

In orthopedics, Ho:YAG laser showed an effectiveness in the ablation of prolapsed discs and in relieving the compression of the nerve root by bone ablation [106]. Charlton et al. compared the ablation on cortical bone of a human femur for both Er:YAG and

Ho:YAG lasers. The thermal damage to the surrounding tissues was around 80 μm with significant charring (~7 μm depth) when Ho:YAG laser was used, which is much larger when compared to 5 μm damaged layer with no charring in the case of Er:YAG laser. However, damage resulting from Ho:YAG laser irradiation was much smaller than the secondary damaged layer produced by CO_2 laser (10.6 μm) that was equal to 200 μm in depth with significant charring that extended to 300 μm depth [107].

2.5.5 Nd:YAG laser in medicine

Neodymium-doped, yttrium aluminum garnet (Nd:YAG) laser has 1.064 μm wavelength, which is poorly absorbed by water and hydroxyapatite. This wavelength corresponds to 1.17 eV photon energy, which has the ability to break the chemical bonds of tissue by multiphoton absorption. Nd:YAG laser removes only the superficial layer of the heated tissue and leaves the rest of the tissue chemically altered. B. Gasˇpirc and U. Skaleric's study showed that Nd:YAG alters the chemical structure of the proteins and results in thermally damaged root surface for the dental tissue [99]. The thermal damage results from Nd:YAG ranging from heat cracking to charring. However, cooling with air or water during ablation can reduce the damage, but 25- 40% increase in laser energy will be required for equivalent ablation effect [108].

Nd:YAG irradiation has 10 times greater absorption in oxyhemoglobin than in water [109], hence it shows effective results in legs veins such as spider vessels [110].

2.6 Lasers in some orthopedics procedures

Arthroscopy: This is a minimally invasive surgical procedure, where a small incision is created to insert a camera for joint diagnosis, or any other mechanical/electrical instrument for joint treatment, such procedures are very common in shoulder and knee joints [111]. Jackson who is considered the father of arthroscopy became interested in lasers in the early 1960s. In 1981 Whipple introduced his results of CO_2 laser assisted arthroscopies [112], in the same time, other studies used Nd:YAG laser (1.064 μm, 15 - 40 Watts) as an arthroscopic tool in different orthopedic procedures such as menisectomy, where the torn part of meniscus is removed, and chondroplasty in which the cartilage of the joint is reshaped or repaired. The results showed normal healing, short recovery period, and lower swelling and pain when compared to mechanical instruments, which suggests that lasers have the potential to be used as an arthroscopic removal instrument [113, 114]. In the mid of 1980s the pulsed CO_2 laser (10.6 μm) was approved by FDA to be used in meniscectomy in USA hospitals. Brillhart carried out an arthroscopy procedure in 1992 using Nd:YAG (1.44 μm) which showed comparable effects to Ho: YAG laser (2.1 μm) that was developed especially for arthroscopic surgery in the late 1980s. Other types of laser such as KTP, Er:YAG, and excimer were tested in later studies for its potential to be used in the arthroscopy. However, Ho:YAG remains the most accepted laser for this application so far [112].

Spinal Surgery: Open operations used to be followed for spinal surgeries. Recently, researchers attempted to find less invasive procedures to avoid postdiscectomy syndrome (failed back), which results from some open procedures, such as spinal disc decompression surgeries, where a small portion of bone that exists over a nerve root is removed to give larger space for the nerve [112]. Other types of spinal surgeries can be performed, such as spinal osteoid osteomas removal, where the painful lesion that exists in the vertebral body is removed [115]. Later studies evaluated the feasibility of several types of lasers in spinal surgery such as CO_2, Er:YAG, KTP, Nd:YAG, and Ho:YAG lasers. However, KTP, Nd:YAG, and Ho:YAG are now used in intradiscal and endoscopic methods [112].

The feasibility of many lasers, especially those that have near infrared wavelengths, in orthopedic medicine was tested. According to the results, it was believed that Ho: YAG laser is one of the most viable lasers to be used in spinal and orthopedic surgeries [112].

Osteotomy: This is an orthopedic procedure in which bone cutting is involved. This procedure can be carried out in different sites and for different purposes. For example, in knee osteotomy, a wedge of bone near the affected joint is removed to reduce the pressure at this area, while in hip osteotomy, cutting of the pelvic bone is performed to rotate the socket so it can be in a better position in the cases where the socket does not sit properly on the top of the thigh bone [116, 117].

The first laser used to perform osteotomy was CO_2 laser in 1969. The procedure showed less traumatic and more precise results when compared to the mechanical

instruments which were used for this purpose. However, the thermal damage of the surrounding tissues was an obvious limitation. Later studies demonstrated that pulsed lasers reduce this effect of thermal damage. Papadaki et al. examined the feasibility of pulsed Er:YAG laser (300 μs, 0.5-2 J/pulse) to perform vertical ramus osteotomy in pig mandibles, where the results showed a smooth and free-carbonization cutting [118].

Chapter 3: EXPERIMENTAL CHARACTERIZATION OF ABLATION PARAMETERS

The first section of this chapter covers the experimental method that was used for all experiments. It describes the laser system set-up, ablation protocols, and laser parameters that were chosen for each experiment. Different characterization methods were used to analyze the ablated samples. These methods will be also discussed in this section.

The second section will discuss the first part of the experiments: the characterization of ablation parameters where a series of experiments was carried out to investigate the ablation characteristics of cortical bone.

3.1 Experimental method

The following sub sections are an overview of the experimental setup used in ablation, bone samples, and data analysis process.

3.1.1 Experimental setup

The experiments were carried out using a customized ultrafast laser machining system. The pump laser is a high power continuous wave, frequency doubled neodymium doped yttrium orthovanadate (Nd: YVO_4) laser (Millenia V, Spectra Physics) which has a wavelength of 532 nm. This laser was used to pump the other laser, Titanium: Sapphire mode-locked oscillator laser, also known as Ti: Al_2O_3 laser (Tsunami, Spectra Physics), which has output of 780 mW, and generates pulses with 90 fs pulse duration, ~10 nJ maximum pulse energy, and 83 MHz repetition rate. A fiber- coupled spectrometer

(PC200, Ocean Optics) was used to measure the laser peak wavelength before entering the chirped-pulse amplifier (CPA). These pulses then seeded the CPA (Spitfire, Spectra Physics) where the incoming pulse is stretched in time by using dispersive optics and then amplified and recompressed by a compressor, to generate amplified short pulses. The generated pulses have energy of ~325 μJ (with maximum power of 400-500 mW), 170 fs [Full Width Half Maximum (FWHM)] and 1 kHz repetition rate. Ti: Sapphire crystals have absorption band at 400-600 nm, and emit wavelength centered on 800 nm. The beam generated from the CPA had a near-Gaussian intensity profile; the initial diameter of the beam was ~10 mm which was reduced by beam condenser to be ~4 mm in diameter. The CPA is pumped by a diode-pumped Nd: yttrium-lithium-fluoride (Nd:YLF) laser source (Evolution X, Spectra Physics) with a wavelength of 527 nm and 1 kHz repetition rate.

Fig.15 shows a schematic description of laser ablation setup. That follows the laser irradiation path starting from the CPA until the laser reaches the sample.

The pulse energy was adjusted using a combination of a half wave plate (0RP44-3, Newport) and a thin film polarizer (11B00UP.26, Newport). A photodiode (DET210, Thorlabs) was used to calibrate the laser beam at different half-wave plate positions. A computer controlled mechanical shutter (VS25S2S1, Uniblitz) was used to control the exposure time.

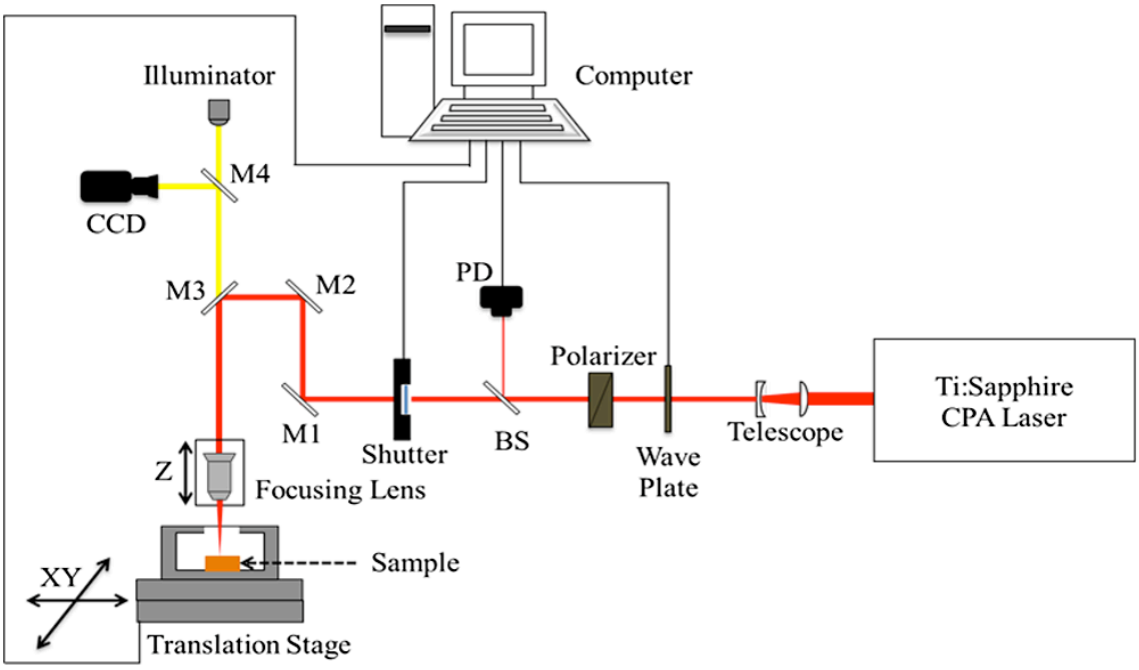

Figure 15: Schematic description for laser ablation setup; after the amplification of the laser pulse energy (in CPA stage). The laser energy is adjusted through changing the beam polarization by a combination of wave plate and polarizer, and then a portion of the beam is directed to the photodiode by beam splitter for calibration. The output is read by a computer which controls the shutter. The beam goes through some mirrors: M1 and M2 (reflected mirrors), M3 (dichroic mirror), and M4 (beam splitter) [119]

After that, the collimated beam was directed to a plano-convex lens (f = 12.5 cm, BK7, Thorlabs). This lens focused the beam to $1/e^2$ of peak intensity, at which the spot size diameter ($2\omega_0$) is equal to 30.2 μm, where ω_0 is the beam waist.

The depth of focus (also called confocal parameter, b), is the distance between two points along the propagation direction of the beam where the area at the confocal positions is twice the area at the beam waist ($2\omega_0$), as shown in Fig.16. It was calculated for an 800 nm wavelength to be 1.8 mm, assuming Gaussian beam profile, according to the following equation [120]:

$$b=2Z_R=\frac{\pi\omega_0{}^2}{\lambda} \quad (4)$$

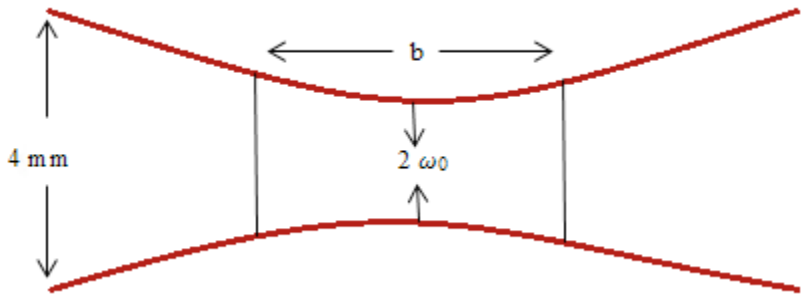

Figure 16: Gaussian beam propagation; the beam waist (minimum spot diameter) was found to be 30.2 µm, and the confocal parameter (distance of two points where the area is twice the area at the beam waist) was calculated to be 1.8 mm

The steel chamber in which the samples were placed was mounted onto a computer controlled X-Y translational stage (UTM100PP.1, Newport). The focusing lens was mounted on a Z translation stage (MFN25PP, Newport) for laser focal point adjustment along the Z direction. The ablation process was monitored using a confocal monochrome charged-couple device (CCD) camera, and white LED light source was for illumination purpose.

An autocorrelator was used to measure the pulse duration prior to each experiment. Fig.17 shows the schematic of Michelson interferometer based autocorrelator, where the pulses are divided into two paths by beam splitter. One of them is directed to a mirror on a motorized translational stage which creates an optical delay. After that the two beams are recombined and steered to the frequency-doubling crystal. The intensity of the generated frequency-doubled photons is measured by photodiode. From this measurement, we can estimate the pulse duration because the photons intensity is a function of the overlapping of the two pulses.

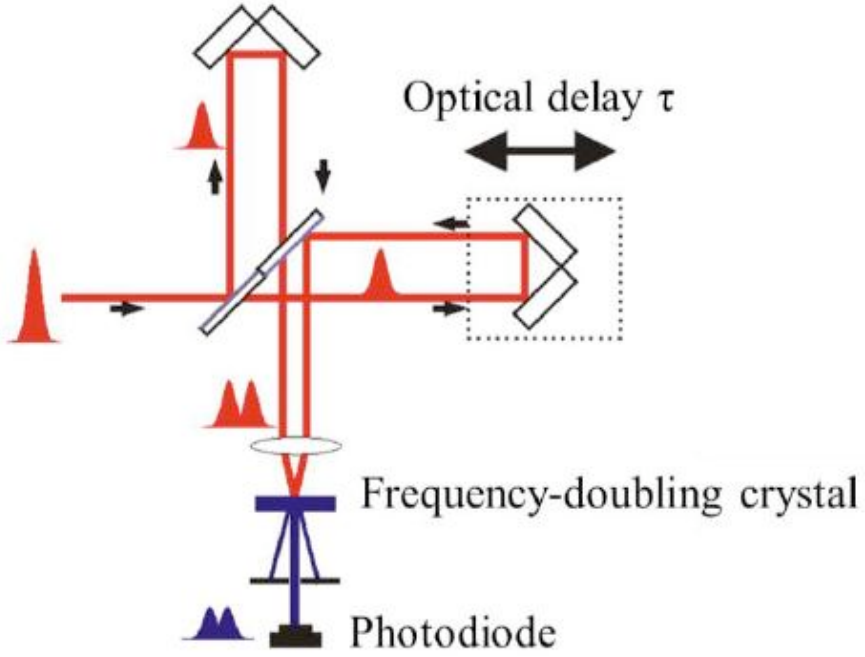

Figure 17: Schematic of autocorrelator that is based on the Michelson interferometer principle. Autocorrelator was used to measure the pulse duration prior the experiments. The beam is split into two portions, one of them is delayed by a mirror, after that the two beams are recombined and the frequency produced by the crystal is measured by the photodiode, and thus the pulse duration can be deduced. Reprinted with permission from [121]

After the optical alignment, and beam profile and pulse duration measurements, power calibration was carried out as a last step of beam diagnostic procedure. Power calibration was performed by reflecting a small portion of the laser beam onto a photodiode (DET 210, Thorlabs) using a pellicle beam-splitter (PBS). The photodiode was calibrated using a power meter which was placed in the beam path to measure the laser power after passing the optical components. After the calibration, the power meter was removed and the photodiode was used to measure the incident laser power.

Fig.18 is the beam profile measured before the ablation process, it has a Gaussian distribution with some fluctuations as shown in the profile, which might be due to dust on the optics, or might indicate damaged optical elements.

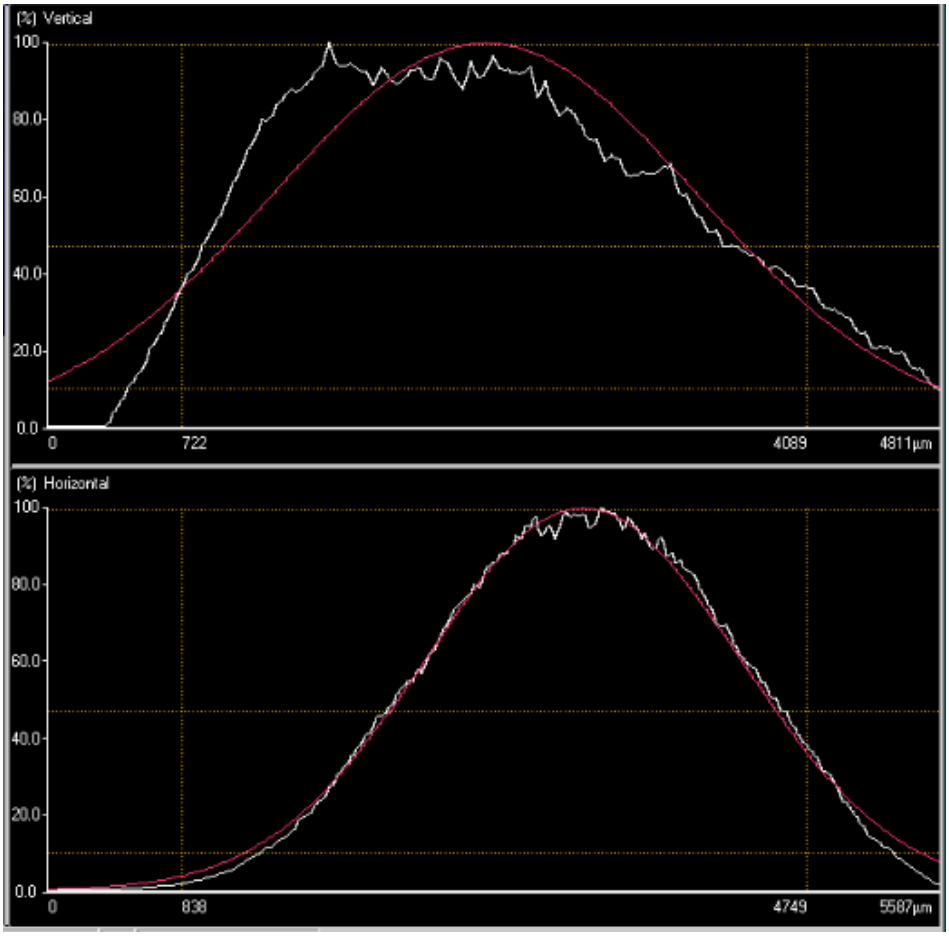

Figure 18: Beam profile measured by CCD camera before the experiments; it shows the actual beam intensity in the vertical (top) and horizontal (bottom) directions, the red curve presents the theoretical Gaussian profile

3.1.2 Bone samples

The use of animal tissue and the experimental protocol was approved by the McMaster Animal Research Ethics Board. Bone samples acquired from a local butcher in Hamilton, Ontario, were vertebral bones taken from immature pigs.

Tweezers were used to remove the soft tissue and periosteum from the bone surface. After that the vertebral bones were cut into cubic samples, as shown in Fig.19, using a

slow-rotation, diamond-blade precision sectioning saw (IsoMet, Buehler), the samples were 10 mm in length and width, and 5 - 8 mm in height. Both cortical layers (~1- 3 mm thickness) and the trabecular bone (~5 mm thickness) were included in the sample. The samples were kept with unpolished surfaces to try to mimic the in vivo environment.

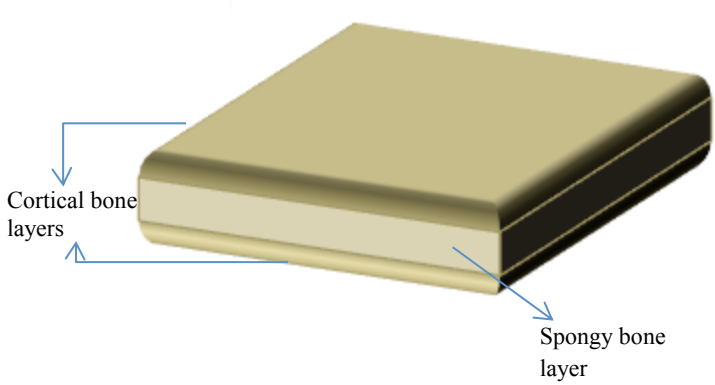

Figure 19: Bone sample that shows two layers of cortical bone sandwiching the cancellous bone layer. In our experiments, the sample was ~10 mm in length and width, and ~5-8 mm in height; the cortical layer was ~1-3 mm thickness, while cancellous was ~5 mm thickness

The samples were treated by laser directly after sectioning, and then they were kept in the freezer in 10% formalin solution until the scanning process.

All the samples were ablated within a sealed drilling vial, consisting of a glass container with a plastic lid. A small circular hole (~20 mm diameter) in the lid was covered by a glass slide (~25 mm diameter, 0.13- 0.17 mm thick) which acts as a window for the laser beam. The slide was sealed in the lid using commercially-available transparent epoxy adhesive. Paraffin wax was used to fix the samples in the bottom of the

vials. After the ablation process, the drilling vials were opened in a fume hood. Fig.20 shows an example of bone sample that was fixed in a drilling vial.

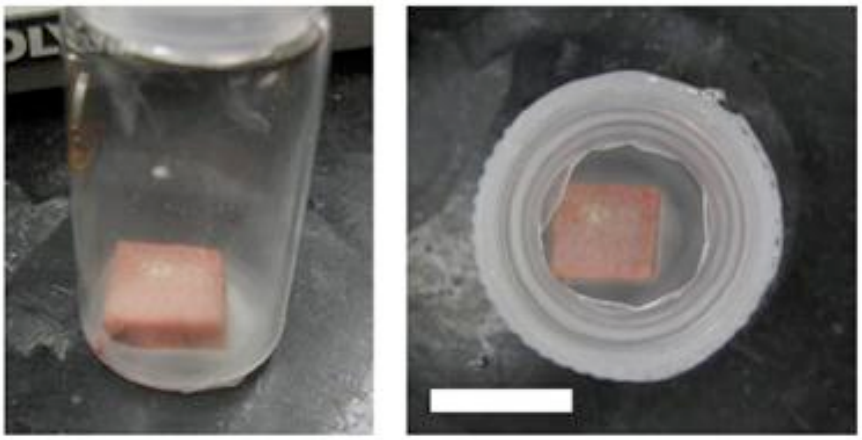

Figure 20: Side view of the drilling vial, that shows the sample attached to the bottom of the vial by paraffin wax (left), and top view of the vial shows the ~20 mm diameter circular hole was created in the plastic lid and covered by glass slide with ~25 mm diameter (right). The scale bar is 10 mm. Reprinted with permission from [121]

3.1.3 Characterization methods

Different techniques were used to characterize the ablation results, these techniques will be discussed in this section of the thesis.

Linear scanned channels were created on the bone surface (see Fig.21) to examine ablation parameters such as ablation depth and removal rates. These ablated samples were cut perpendicular to the channels by diamond-blade sectioning saw (IsoMet, Buehler) into slices with thickness of 700-850 μm. The blade has a thickness of 0.3 mm. Ethanol was used to cool this blade during cutting. These histological slices were covered by cover slip glass and imaged using the microscope described below.

A detailed discussion of the parameters used in the characterization and the results will be presented in the next section.

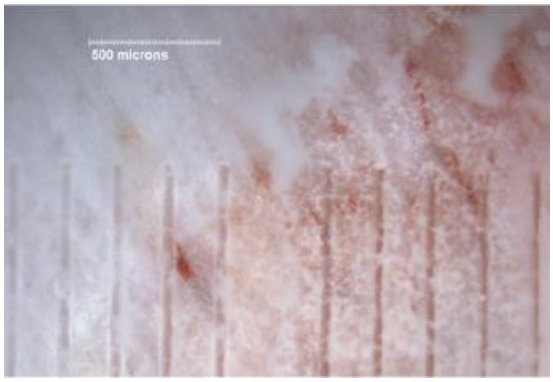

Figure 21: Linear channels were scanned on the bone surface, in order to examine some ablation parameters. The samples after that were cut along their cross section to the channels into slices to be observed by microscope. Reprinted with permission from [121]

Some studies used hematoxylin and eosin to stain the bone samples before microscope examination in order to detect the defects that were produced by laser [122]. Other studies used alkaline phosphatase protein, which was added to the samples prior the laser treatment. This protein denatures at 55 ℃, thus it can be used as a marker for laser heat deposition within the tissue [123].

The reflected-light microscope (Axioplan 2, Zeiss) in the Canadian Centre for Electron Microscopy (CCEM) at McMaster University was used to investigate the ablated lines on the bone surface and to see the edges of the ablated holes. The analyses were carried out using image analysis software (Northern Eclipse™).

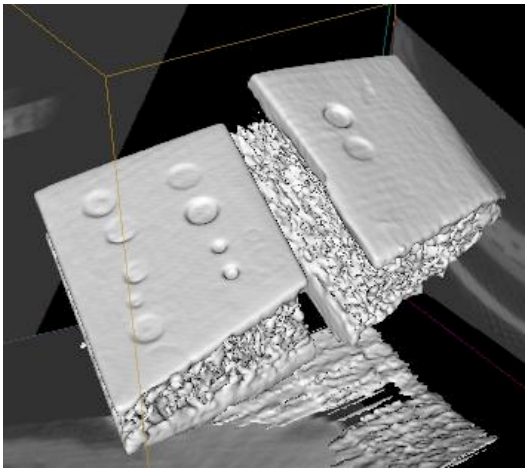

Figure 22: 3D image for two bone samples were scanned in the micro-CT, the 3D reconstruction was performed using Microview program

A micro computed tomography (micro-CT) system with a resolution of 21 microns (1209.523 dpi) was used to image the large-scale holes ablated in bone. The micro-CT consists of an x-ray source, x-ray detector which includes 2D photodiode array, and a high precision rotation stage. Multiple 2D images for the sample were stored and then reconstructed. Image reconstruction was carried out using commercially available construction software, Microview 3D volume viewer and analysis tool (eXplore MicroView v. 2.0, GE Healthcare), which has the ability to import a sequence of 2D images produced by micro-CT and assemble them into 3D image. As shown in Fig.22. The 2D line measurement property was used to measure the depth and width of the holes. The isosurface application was applied to the hole images to observe the edges of the ablated hole. The micro-CT measurements were conducted at the animal research facility of Guelph University.

3.2 Characterization of ablation parameters

3.2.1 Introduction

Orthopedic procedures require high efficiency, a precise ablation process, and minimal thermal damage to the surrounding tissues. Thermal damage is the main factor of delayed healing of bone, so studies paid attention to this effect and tried to minimize it. Thermal confinement of laser energy can limit the thermal diffusion to the surrounding tissues, which results in higher temperature within the ablated volume. Stress confinement, where tensile stresses are confined in a very small area, is another important factor, as the consideration of this confinement can reduce the energy density required for ablation [73]. These confinements are the key to achieve high ablation efficiency. Researchers tried to increase the ablation efficiency and to confine the laser energy within a very thin layer of tissue, using several strategies such as: (1) decrease in pulse duration of incident laser, allowing energy to be delivered quickly into tissue thus giving the thermal energy a short time for diffusing into the tissue, (2) wavelength strongly absorbed by the target, so lasers were being developed for strongly absorbed emitted radiation, such as far UV and near IR wavelengths, (3) cooling the tissue by water/air spray, and (4) reduce the scanning time of the laser to avoid the cumulative thermal effects [90, 92].

Ultrashort laser (<10 ps) ablation is considered to be a promising tool in orthopedic procedures since it ablates hard tissue by plasma mediated mechanism. This has the benefit of producing precise ablation results, and minimal thermal damage to the surrounding tissues. However, some studies showed that using ultrashort laser results in

lower tissue removal rate when compared to long pulses. For example, Armstrong et al. found from their experiments on ossicular tissue using Ti:Sapphire (1053 nm, 350 fs) that the ablation rate was just 1 um/pulse. This is slow when compared to the ablation rates produced by long pulse lasers that were demonstrated in other studies [124].

Some experiments were carried out in this study to characterize some laser parameters such as pulse energy, scanning speed, pulse duration, and number of scanning passes. A good understanding for the effect of laser parameters on the ablation process leads to the ability to devise proper laser parameters and drilling strategies to optimize the ablation efficiency. These experiments and results will be presented in this chapter.

3.2.2 Ablation threshold

Ablation threshold is the fluence that is required to induce a critical density of the free electrons in the conduction band, at which electrostatic forces can be created that have the ability to break down the material [125]. These forces should be able to destroy the extracellular matrix (ECM) of the ablated tissue rather than only tissue dehydration [38]. In other words, ablation threshold is the minimum fluence (energy per unit area) needed to cause the minimum collateral damage in the tissue [126].

The value of ablation threshold is considered the most important observation during ablation, since it is the key parameter for characterization of the interaction between the laser and tissue [78]. The study of ablation threshold under different laser parameters can provide the precise knowledge of the ablation mechanism [127].

There are several methods for ablation threshold determination; one of them is the D^2 method, in which the relation between the etch diameter and the laser exposure should be found. The intersection of the extrapolation with the abscissa is the ablation threshold.

$$D^2 = 2{\omega_0}^2 \ln(\frac{\emptyset_0}{\emptyset_{th}}) \quad (5)$$

Vogel et al. showed another method to determine the ablation threshold by using the extrapolation of the data for the etch depth versus incident radiant exposure, as shown in the figure below. The ablation threshold in this case is the intersection with the abscissa of the extrapolation [38].

Another method is to measure the appearance of recoil stresses that connected with the removal of tissue material using piezoelectric. High-speed photography was also used to determine the onset material removal in the case of microsecond laser pulses [38]. Optical coherence tomography (OCT) [128], scanning electron microscopes (SEM) [129, 130], and optical microscopes were used in some studies to observe the surface modification with irradiation [131].

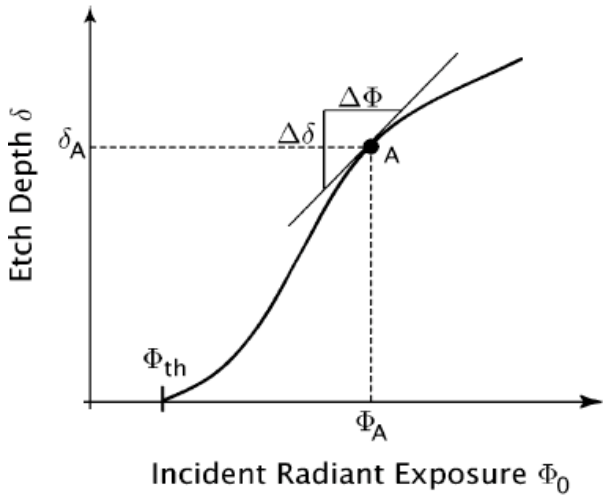

Figure 23: Method to find ablation threshold: the relation between etch depth and incident radiant exposure; the ablation threshold equals to the intersection of the abscissa. Reprinted with permission from [38]

It is preferable to keep the ablation threshold as minimum as possible, that will reduce the collateral damage of the surrounding material [78]. Several studies tried to reduce the ablation threshold. It was found that the ablation threshold depends on some laser parameters such as wavelength [78, 79] pulse duration [126, 132, 133].

For example, Olivié et al. tested the influence of wavelength on the ablation threshold of porcine corneal stroma, by applying wavelengths in the range of 800 nm-1450 nm with 100 fs pulse duration. It was found that the ablation threshold increases from 1.5 J/cm^2 at 800 nm to 2.2 J/cm^2 at 1000 nm, after that the data tends to be saturated for wavelengths longer than 1000 nm. Fig.24 displays these results [78].

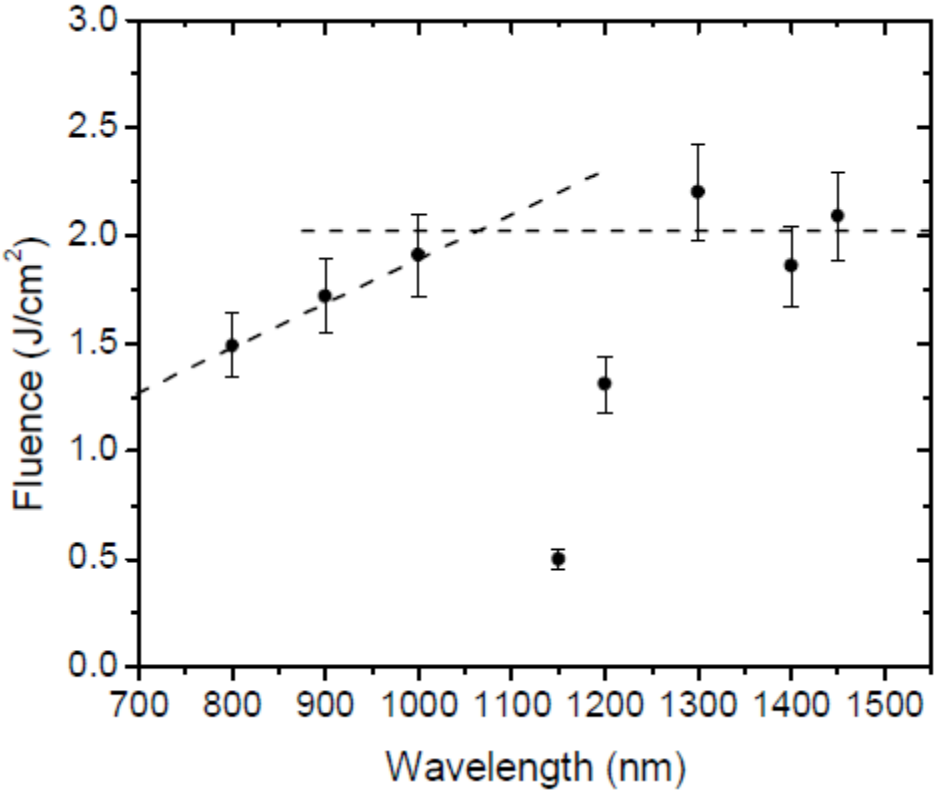

Figure 24: Measured ablation thresholds for corneal stroma at different wavelengths with fixed pulse duration of 100 fs. Reprinted with permission from [78]

These results agree with Jia et al., who found the ablation threshold as a function of wavelength, when fused silica and CaF_2 crystals were ablated by femtosecond laser with wavelength in the range of 250 nm to 2000 nm [79].

Kim et al. studied the pulse duration influence on the ablation threshold of human dentin, which was ablated by a Tsunami laser (800 nm) with different pulse durations in the range of 130 fs to 10 ps. It was found that the threshold increases from 0.75 J/cm^2 for 130 fs up to 3.8 J/cm^2 for 20 ps (which is around 4 times the threshold at 130 fs) [131]. Their results agree with what has been demonstrated in a study for Stern et al., who found

that the ablation threshold of bovine cornea decreases with using smaller pulse durations. Whereas the threshold was 50 μJ for 30 ps pulses, this value was lowered to 10 μJ when 1ps pulses were used, and with further decreasing in pulse duration to 100 fs, the ablation threshold reached to 2.5 μJ [133].

The ablation threshold is different for each biological tissue, even if they are ablated using the same laser parameters because they have different properties. Murray and Dickinson have studied the ablation threshold for different biological tissues (enamel, dentin, chicken flesh, and chicken bone) which were ablated by XeCl laser (308 nm) with 5 Hz repetition rate and 200 ns pulse duration. It was found that the enamel has the highest ablation threshold which was 2.86 ± 0.01 J/cm^2, followed by the dentin which was 0.5 ± 0.01 J/cm^2, the soft tissue has 0.3±0.01 J/cm^2 threshold, and the lowest was for the chicken bone 0.1 ± 0.01 J/cm^2 [134]. Other study for Loesel et al. found that enamel has ablation threshold of 10 J/cm^2 when ablated by dye laser (630 nm, 1 kHz) with pulse duration of 35 ps. This threshold was reduced to 1.1 J/cm^2 when the pulse duration decreased to 100 fs. The ablation threshold for bovine brain tissue was 20 J/cm^2 at 35 ps, which is much higher when compared to the ablation threshold of enamel (1.5 J/cm^2) at 100 fs [135]. The table below summarizes the data described in this paragraph.

Table 5: Summary table for ablation threshold values for different tissues using different lasers

Tissue	Laser	Pulse duration	Ablation threshold
Bovine brain	Dye laser (630 nm)	35 ps	20 J/cm^2
Enamel	Dye laser (630 nm)	35 ps	10 J/cm^2
Enamel	XeCl (308 nm)	200 ns	2.86 ± 0.01 J/cm^2
Bovine brain	Dye laser (630 nm)	100 fs	1.5 J/cm^2
Enamel	Dye laser (630 nm)	100 fs	1.1 J/cm^2
Dentin	XeCl (308 nm)	200 ns	0.5 ± 0.01 J/cm^2
Chicken flesh	XeCl (308 nm)	200 ns	0.3±0.01 J/cm^2
Chicken bone	XeCl (308 nm)	200 ns	0.1 ± 0.01 J/cm^2

3.2.3 Ablated groove depth vs. pulse energy

3.2.3.1 Method

Bone samples were ablated using 170 fs pulse duration and 1 kHz repetition rate laser parameters. Multiple lines were created on the bone surface with increasing fluences in the range of 5 to 20 J/cm^2. The channels were 7000 μm long and separated by 200 μm space. Different scanning speeds of 100, 250 and 500 μm/s were used to ablate the channels. For each sample, at a specific scanning speed, several channels were created using different laser fluences in order to investigate the groove depth as a function of pulse energy at each scanning speed.

The samples were cut cross sectioned to the grooves using diamond-blade sectioning saw into slices 700-850 μm thick. After that, the grooves were observed using reflected light microscopy, and a plot of groove depth as a function of laser fluence was established at various scanning speeds.

3.2.3.2 Results and discussion

Fig.25 is a microscope image of cross sectional slices showing the side-view of the ablated lines, which are created by 100 µm/s scanning speed (Fig.25 a) and 500 µm/s scanning speed (Fig.25 b) at different laser fluences in the range of 5 to 20 J/cm^2.

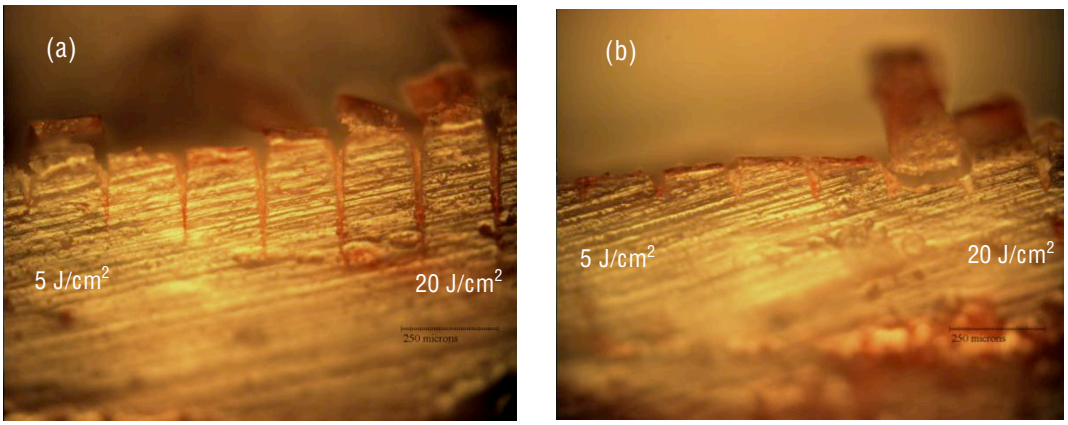

Figure 25: (a) ablated grooves at different laser fluences in the range of 5 to 20 J/cm^2 and fixed scanning speed of 100 µm/s; (b) ablated grooves at different laser fluences in the range of 5 to 20 J/cm^2 and fixed scanning speed of 500 µm/s

From the cross sectional slices, the depth of the groove was measured from the surface of the bone to the deepest apparent deformed point, as shown in Fig.25.

The results showed that the groove depth increases logarithmically with the increase of the laser fluence for all the scanning speeds (Fig.26). Another observation was that the grooves ablated by slower scanning speed have greater depths when compared to those which were scanned faster. This can be explained by the number of pulses effect, where lower speeds allow more pulses at each spot. This phenomenon is described in detail in the next section.

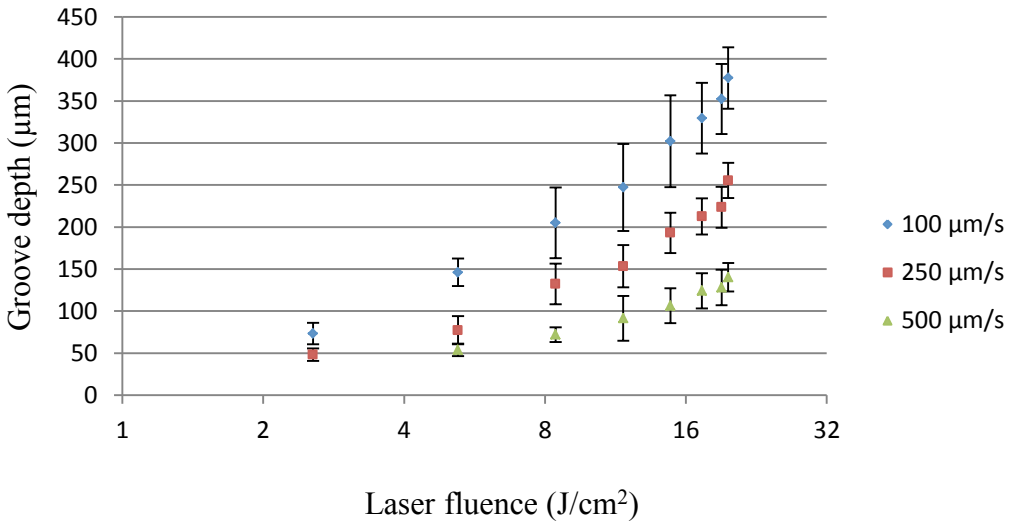

Figure 26: Plot shows the groove depth as an exponential function of laser fluence at different scanning speeds

From the figure above we can see that the difference between depth values at different scanning speeds increases with the laser fluence. The depth values at low fluence are almost the same for all scanning speeds. Assuming Gaussian beam distribution with a peak fluence of $\emptyset_0$ (Fig. 27), the depth of the ablated grooves can be calculated as:

$$d = d_0 \ln\left(\frac{\emptyset_0}{\emptyset_{th}}\right) \quad (6)$$

Where d_0 and $\emptyset_{th}$(ablation threshold) are the fitting parameters.

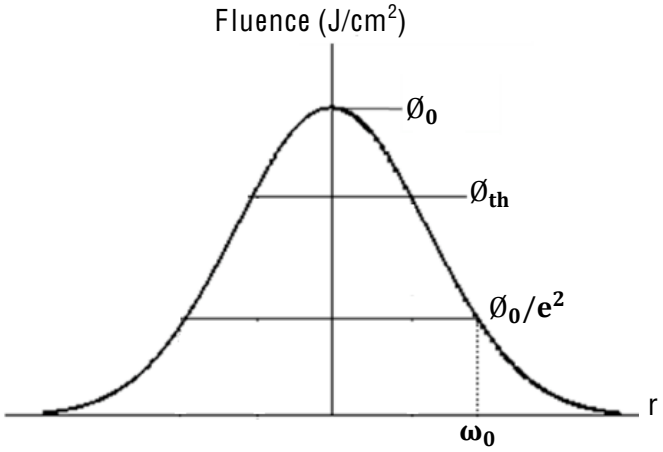

Figure 27: Gaussian beam distribution demonstrates the laser fluence as a function of beam radius; the laser fluence is equal to $Ø_0/e^2$ at the beam waist (ω_0)

The parameters (d_0 and $Ø_{th}$), that were extracted from depth versus fluence plot, are summarized in table 6:

Table 6: The fitting parameters of different scanning speeds (100, 250, and 500 µm/s)

Scanning speed (µm/s)	d_0 (µm)	φ_{th} (J/cm^2)
100	144.96	1.78
250	97.464	1.95
500	62.997	2.48

From the previous table, we can see that the ablation threshold has a direct relation with the scanning speed. These results showed an agreement with what was found in previous work (Emigh et al.) [136]. Table 7 shows the ablation threshold at different scanning speeds that was found in the previous work [136].

Table 7: The ablation threshold at different scanning speeds; the ablation threshold was measured using D^2 method [136]

Scanning speed (µm/s)	φ_{th} (J/cm^2)
1208	2.37
604	2.36
403	2.28
302	1.72
100	1.66
60	1.69
30	1.75

This can be explained by a phenomenon called the incubation effect, in which the ablation threshold is reduced due to the damage accumulation effect resulting after irradiation by multiple pulses [137]. The incubation can be noticed as more pulses are delivered. This was demonstrated by Lim et al. who observed larger width of holes ablated in bovine bone as increasing number of applied pulses [138].

In an experiment by Girard et al., pig mandible cortical bone was ablated using a 775 nm wavelength and 200 fs pulse duration, they found that the ablation threshold was 0.69 ± 0.08 J/cm^2 when 225 pulses/spot were applied under 200 µm/s cutting speed and 1 kHz repetition rate [129]. This threshold is lower than what we achieved at the same and greater number of pulses per spot although the parameters used were comparable. The reduction in ablation threshold maybe resulted from the polished bone samples used in their experiments. Girard used the same laser parameters mentioned before to find the ablation threshold of cortical bone at 387 nm wavelength, which was reduced to 0.19 ± 0.05 J/cm^2 [129].

3.2.4 Ablated groove depth vs. scanning speed

3.2.4.1 Method

Another important laser parameter, the scanning speed, was characterized. The effect of scanning speed on the groove depth was investigated. Linear channels, with 7500 μm length and 200 μm separations between the channels, were ablated on the surface of porcine samples using 170 fs pulse duration, 1 kHz repetition rate laser parameters. For this experiment, two different laser fluences (10.33 and 19.55 J/cm^2) with 10 different levels of scanning speed in the range of 100 to 1000 μm/s (100 μm/s increment) were used. Samples were cut cross-sectioned to the ablated channels into thin slices. Reflection microscopy was used to examine these slices.

The scanning speed determines the number of incident pulses that are delivered to the sample. The effective number of incident pulses can be calculated according to the following equation:

$$N_{eff} = \sqrt{\frac{\pi}{2}}\,\frac{\omega_0 f}{v} \tag{7}$$

Where N is the number of incident pulses, v the scanning speed, and f is the repetition rate.

Table 8 shows the incident and the effective number of pulses per spot for different scanning speeds.

Table 8: The fitting parameters of different scanning speeds (100, 250, and 500 µm/s)

Scanning speed (µm/s)	N_{eff}	φ_{th} (J/cm^2)
100	189.20	1.78
250	75.68	1.95
500	37.84	2.48

3.2.4.2 Results and discussion

Fig.28 is a microscope image of the cross-sectioned slices. It shows a side- view of grooves that are ablated using 10.33 J/cm^2 laser fluence (Fig.28 a), and 19.55 J/cm^2 laser fluence (Fig.28 b) at different scanning speeds in the range of 100 to 1000 µm/s.

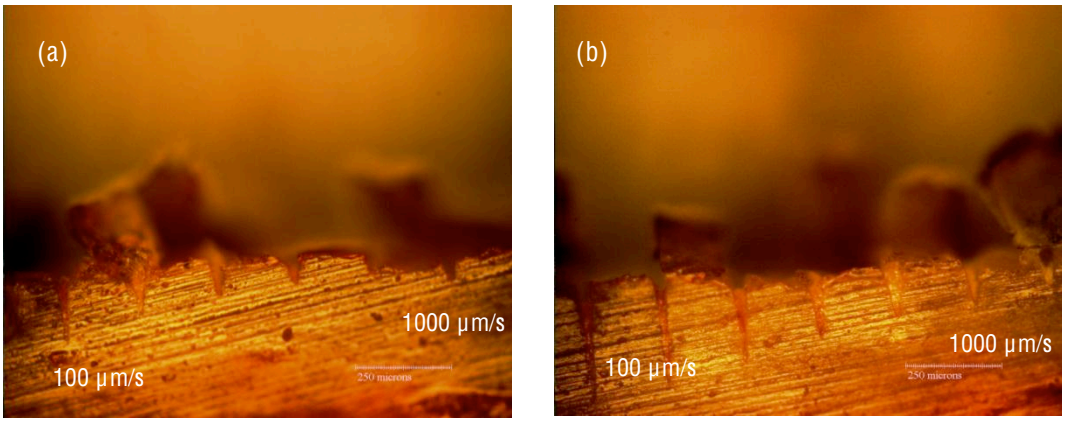

Figure 28: (a) ablated grooves at different scanning speeds in the range of 100 to 1000 µm/s and fixed laser fluence of 10.33 J/cm^2; (b) ablated grooves at different scanning speeds in the range of 100 to 1000 µm/s and fixed laser fluence of 19.55 J/cm^2

It was observed that the depth of the ablated groove increases with the reduction of the scanning speed, because there are more incident pulses per spot delivered at lower speeds. Another observation was that those grooves ablated by higher laser energy have greater depths due to the higher energy deposited in each spot at greater laser energies.

Fig.29 illustrates the groove depth as a function of scanning speed at two different laser fluences. The difference between the two relations is significant at low scanning speeds, while at higher speeds the relation seems to be almost the same for both fluences. This observation indicates that using slower speeds (with larger number of pulses) results in a higher ablation efficiency, and that the relationship depends on the laser fluence.

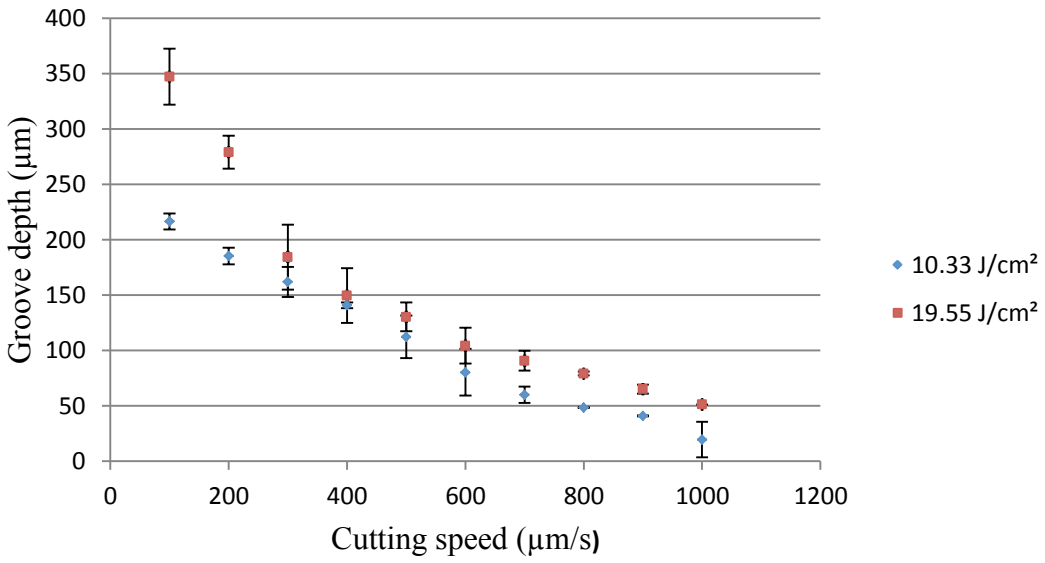

Figure 29: Plot shows the groove depth as function of scanning speed at two different laser fluences 10.33 J/cm^2 and 19.55 J/cm^2

At higher speeds the ablation efficiency does not seem to be significantly affected by the laser fluence. Since at high speeds, the effective number of pulses is low, this leads to low energy deposition within the tissue and thus less tissue removal. Lower speeds allow more pulses to deposit their energy into tissue, and it might give debris enough time to move away, producing larger depths as a result.

Another plot (Fig. 30) of the removal rate versus scanning speed was established. The whole depth of the groove was divided by the number of pulses to get the depth per pulse, or what is called the removal rate.

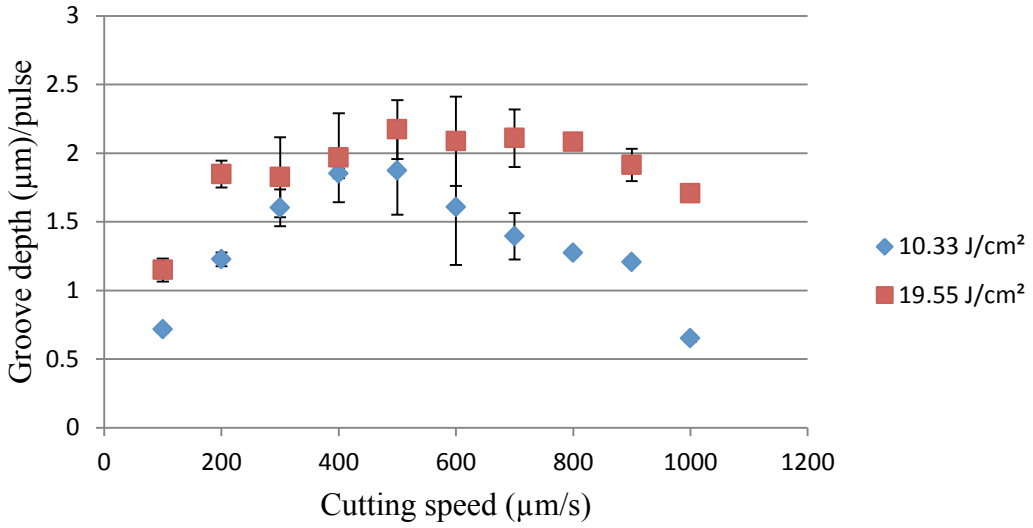

Figure 30: Plot shows the depth per pulse as function of scanning speed at two different laser fluences 10.33 J/cm^2 and 19.55 J/cm^2

It was found that the depth per pulse increases with the scanning speed until a maximum value somewhere between 500 and 800 μm/s, after which it starts decreasing. Debris accumulation in the bottom of the grooves has been suggested as an explanation for this behavior. Since debris can act as a shield that may hinder the progress of the ablation and lower the ablation rate at higher scanning speeds.

Successive intense short pulses with fluences lower than the threshold can lead to accumulated thermal stresses, which cause accumulation of defects and thus ablation at lower laser energy. This may have the advantage of reducing thermal damage in the surrounding tissues.

This effect can be characterized by the incubation effect coefficient (ξ), which can be calculated using the power equation:

$$\emptyset_{th}(N) = \emptyset_{th}(1) \text{ x } N^{\xi-1} \quad (8)$$

Where $\emptyset_{th}(N)$ the threshold of N pulses, $\emptyset_{th}(1)$ is single pulse ablation threshold, and N x $\emptyset_{th}(N)$ is the accumulated fluence. This equation was basically developed for metals and semiconductors, under ultrashort laser ablation.

From N x $\emptyset_{th}(N)$ versus N plot, the slope represents the incubation coefficient, and the y-intercept represents $\emptyset_{th}(1)$.

The degree of the incubation (the incubation coefficient) indicates the change in ablation threshold when the number of pulses increases [121]. It is desirable to keep the ablation threshold as low as possible, in order to reduce the collateral damage of the surrounding tissue [78]. The incubation effect is one of the most effective ways to reduce the ablation threshold.

In our experiments, the results show that the ablation threshold decreases from a maximum of 2.48 J/cm^2 with 500 µm/s scanning speed to 1.78 J/cm^2 with 100 µm/s scanning speed, see table 8. Also, a drop from a maximum of 2.37 J/cm^2 with 25 pulses/spot under 1208 µm/s cutting speed to 1.66 J/cm^2 with 300 pulses/spot under 30 µm/s cutting speed in Emigh's experiments was noticed [136], see table 7.

Other study was carried out by Kim et al. showed the decreasing of ablation threshold when increasing the number of pulses (Fig. 31), in 130 fs ablation of human dentin samples [139].

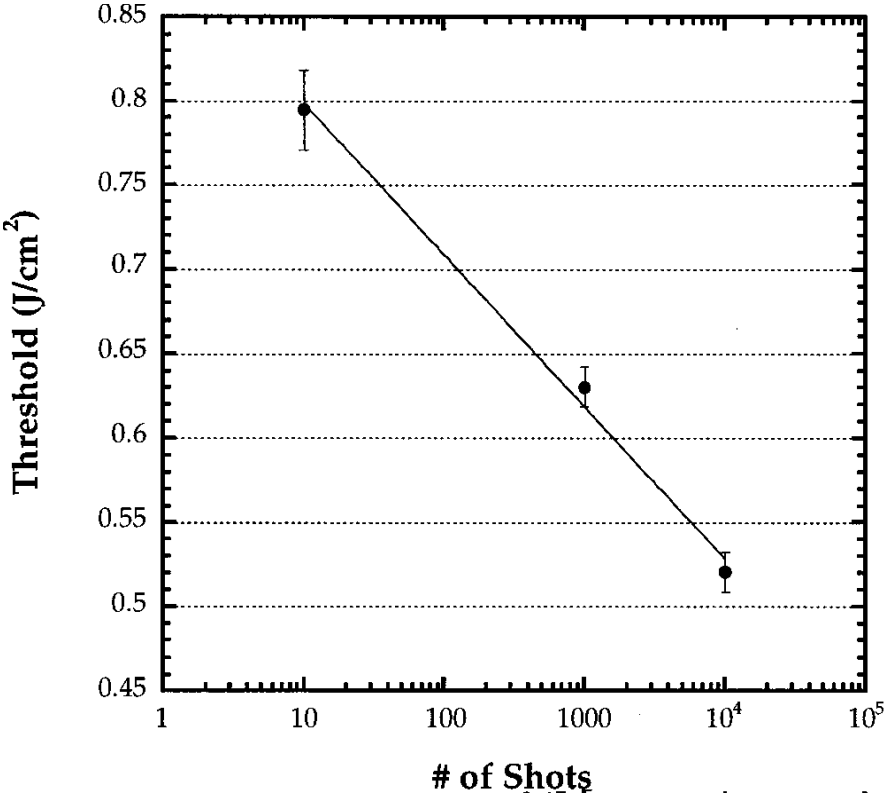

Figure 31: Ablation threshold as function of number of shots for human dentin ablated by 130 fs pulses. Reprinted with permission from [139]

3.2.5 Ablated groove depth vs. number of consecutive passes

3.2.5.1 Method

Several passes over the same place is required sometimes to attain the desired depth, when it may not be achieved with a single pass. The effect of number of consecutive passes on the groove depth was examined. Channels of 7500 μm long were created on the surface of porcine bone sample with 200 μm space between the channels. The laser parameters were used in this experiment are 170 fs pulse duration, 1 kHz repetition rate

and 10.33 J/cm^2 laser fluence. Multiple pass scanning (1, 5, 10, 50, and 100 passes) were carried out over each line using a fixed scanning speed of 500 µm/s. Using the diamond blade saw, the samples were cut cross-sectioned to the ablated channels into thin slices. These slices were examined using reflected light microscopy.

3.2.5.2 Results and discussion

Fig.32 is a microscope image for one of the slices. It shows a side-view of the ablated channels, which are ablated by different number of passes (5, 10, 50, and 100 passes from left to right). Fixed laser fluence of 10.33 J/cm^2 with fixed scanning speed of 500 µm/s was used.

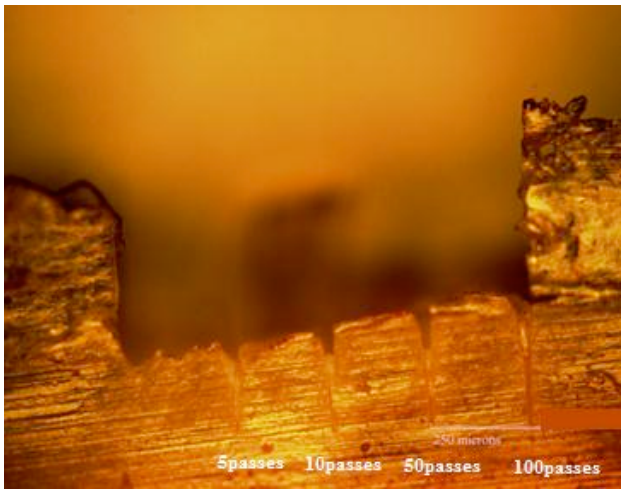

Figure 32: Ablated grooves at different number of consecutive passes with fixed scanning speed of 500 µm/s and fixed laser fluence of 10.33 J/cm^2

As shown in the figure above, increasing the number of passes over the same groove resulted in deeper groove depths. However, increasing the number of passes was accompanied by an increase in the amount of debris accumulated in the bottom of the groove. The groove depth as a function of the number of passes was demonstrated in the plot below (Fig .33):

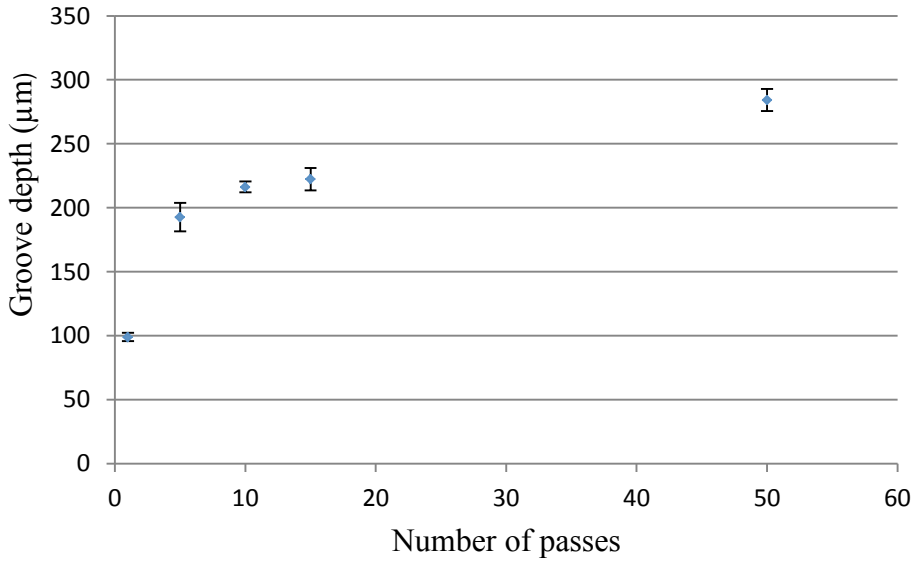

Figure 33: Plot shows the groove depth as function of number of passes at laser fluence of 10.33 J/cm^2 and scanning speed of 500 µm/s

The results showed an increase in the groove depth when the number of passes increases up to 10 passes. After that the rate of depth increasing becomes much lower, because of the energy loss which occurs due to the accumulated debris after a certain number of passes. Another reason for this phenomenon is, since the groove acts as a waveguide for the propagated pulses, increasing of the groove depth due to large number

of passes increases the probability of scattering and absorption during pulse propagation, which reduced the pulse energy, resulting in a lower ablation rate, until the pulse energy becomes below the ablation threshold at the final depth.

Other studies investigated the effect of number of consecutive passes over the same region on the ablation process for different materials. For example, Borowiec (2004) used the same femtosecond machining system that is described in this thesis to ablate indium phosphide. It was found that the groove depth linearly increased with the number of passes over the same groove until 20 consecutive passes. Above 20 passes, the relation deviates from the linear dependence, and the increasing of depths rate was reduced until it reached a limit at 100 passes [140].

However, this reduction in removal rate as the groove depth increases can be compensated by using a different drilling strategy, such as the ablation with multiple passes at variable focus depths as suggested by Emigh [121], where the focal plane of the laser was lowered by 150 μm after each successive pass. The laser parameters which were used in this experiment were 170 fs pulse duration, 250 μm/s scanning speed, and 33.4 J/cm^2 laser fluence. The average increase of the total crater depth was 138.9 μm after every lowering step of the depth of focus. The total groove depth was found as a function of the number of beam focus positions. As shown in Fig.34.

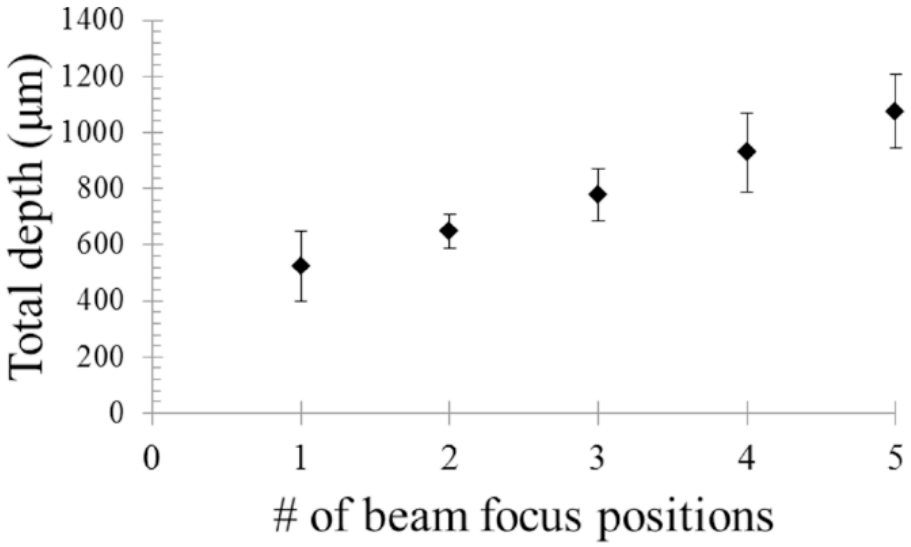

Figure 34: The total crater depth of ablated bone samples as a function of the number of beam focus positions; 1 focus position means that the laser beam focal plane was aligned with the bone surface, the focal plane was then moved downward (in the z direction) by 150 µm for every focus position. Reprinted with permission from [121]

3.2.6 Ablated groove depth vs. pulse duration

Studies paid more attention for laser interactions with soft tissues when compared to calcified tissues, and that maybe because of the probability for irreversible effects such as fractures that might happen to the bone due to its shear and compressive characteristics.

Several studies demonstrate that ultrashort lasers add an important advantage to the tissue ablation, because of their capability to ablate precisely and with no or a very little thermal damage to the surrounding tissues.

Recently, the door was opened to ultrashort laser applications in dentistry, also there are a few publications for ultrashort lasers interaction with other bone tissues such as cortical bone, spine, and skull.

3.2.6.1 Method

Pulse duration is an important parameter for laser ablation, since it determines the mechanism that drives the ablation. In the previous work, the relation between the groove depth and pulse duration was found. Five different laser fluences in the range of 10 - 30 J/cm^2 with 250 μm/s speed, and four different pulse durations of 150 fs, 500 fs, 5 ps, and 10 ps were used to create four channels on the surface of the bone samples, in order to investigate the pulse duration effect at different fluences. Each channel was 6 mm long with a space of 200 μm between the channels. The samples then were cut cross-sectioned to the channels into 600- 750 μm thick slices, which were examined by the microscope.

3.2.6.2 Results and discussion

Fig.35 shows the effect of pulse duration on the groove depth at different laser fluences.

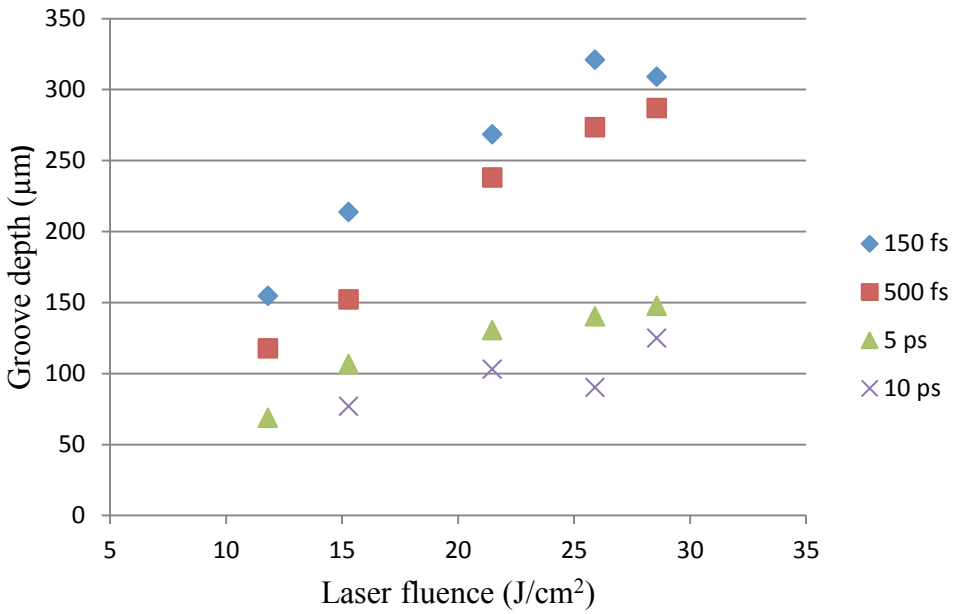

Figure 35: Plot shows the groove depth as a function of laser fluence at different pulse durations (10 ps, 5 ps, 500 fs, and 150 fs)

Fig.35 shows that the groove depth was increasing as a decrease in pulse duration at any fluence value was measured. Smaller pulse durations have higher intensities that result in stronger multiphoton absorption and thus optical breakdown at lower pulse energies. It was found that there is not a great difference in the removal rate for 150 fs and 500 fs laser pulses, however at longer pulses (5 ps and 10 ps) the removal rate was noticeably decreasing. In addition, thermal effects were noticed in samples ablated by 10 ps and 5 ps laser pulses.

Some studies showed that ultrashort pulsed lasers do not alter the chemical properties of bone, which is an important advantage, since it is necessary for bone regrowth after procedure that the chemical properties of bone, such as the relative content of calcium and phosphorus, to remain unchanged [141]. In addition, it was found that ultrashort pulse ablation has the ability to produce a high quality bone cutting in a reasonable procedure time [141]. The ablation mechanism that is initiated by ultrashort pulses is plasma mediated ablation, which is very desirable for surgical ablation because of its high precision [142], and it is also clean process, causing almost no mechanical or thermal damage to the surrounding tissues [21].

Qiu et al. evaluated the feasibility of femtosecond laser (800 nm, 140 fs) in urinary calculi ablation. The results showed that using this pulse duration avoids the risk of thermal accumulation and thus thermal and collateral damage [143].

The necessary intensity that can initiate the plasma formation is ~10^{11} W/cm^2. In nanoseconds regime, that can be achieved by using 1 ns pulses which have fluence of 1 μJ/pulse focused on 1 μm^2 area, which corresponds to 100 J/cm^2. While in femtosecond regime, this intensity can be achieved by using 100 fs pulses with 10 nJ /pulse energy focused on 1μm^2 area and that corresponds to a fluence of 1 J/cm^2. This shows that the total pulse energy in the femtosecond case is a 100 times lower than total energy in the nanosecond case and thus less collateral damage, shockwaves, and bubble expansion will occur using femtosecond ablation [77].

In general and regardless of the ablation mechanism, the laser pulse should be shorter than the time that heat takes to diffuse within the tissue in order to avoid the thermal collateral damage. On the other side, the pulse duration should not be too short which may increase the shock stresses, and which results in mechanical collateral damage [46].

Chapter 4: EXPERIMENTAL MACHINING OF LARGE SIZE HOLES

4.1 Introduction

For successful replacement of mechanical drills with lasers in orthopedic applications, lasers should have the ability to remove bone on a relatively large scale (millimeter to centimeter scales) depending on the application. For example, pedicle screws require holes of ~3 mm diameter and ~30 mm depth [144]. Another example of applications that need large-scale ablation is the artificial implants fixation procedure, where a millimeter scale flat is required. Bone metastases, which are common in spine, pelvis, skull, femur, and ribs, can cause pain and severe functional impairment, such as spinal instability, which has significant impact on the quality of the activities of daily living. Thus, one of the treatment options is the surgical removal for these lesions, where excision of part of bone is required. [145, 146] So, to be considered in orthopedics procedures, lasers should have the ability to cut large-scale sections of bone.

The first part of my experiments investigated the effect of some laser parameters (fluence, scanning speed, pulse duration, and number of passes) on the ablation process in order to achieve the optimal laser ablation. This was considered the first step towards large-scale holes drilling. However, optimized laser parameters are not enough to guarantee optimal hole ablation. When the ablation goes deeper, other factors may contribute to the ablation quality of holes, such as beam scattering by crater walls or reduction of ablation efficiency due to debris accumulation in the bottom of the holes.

Thus, in this chapter, large hole ablation was investigated using two different scanning strategies (same used in our previous work but with different laser parameters): helical scanning and concentric circles scanning. These strategies were used previously by Girard et. al to ablate cortical bone using 775 nm wavelength and 200 fs pulse duration laser parameters [129]. Other experiments were carried out by Lim et al. who created micropillars in bovine cortical bone using concentric circles that were scanned by laser pulses of 150 fs pulse duration, 775 nm wavelength, and 3 kHz repetition rate [138]. The goal of the experiments, listed in this section, is to develop the scanning strategies and try to get large-scale holes in a reasonable machining time.

This chapter presents the experiments we carried out to remove large scale sections of bone tissue using two different scanning strategies: concentric circles scanning and helical scanning.

4.2 Concentric circle scanning

4.2.1 Methods

The bone samples that were used in the large scale scanning were taken from vertebral bone of immature pigs. The experiments were performed using the laser machining setup that was described in chapter 3. The holes were created using a laser beam with pulse duration of 170 fs, 1 kHz repetition rate, and maximum pulse energy of ~400 to 500 μJ.

For this set of experiments, 20 concentric circles were created with 25 µm increment in radius for successive circles, as shown in the figure below. This increment was chosen to achieve a sufficient overlap between the successive circular paths of the laser beam, and since the laser beam spot diameter is ~30 µm then the increment should be less than 30 µm. Once one layer of concentric circles is done, the beam was moved downward 200 µm in the z-direction to create the second layer, and so on, as shown in Fig.36. The number of layers depends on the crater depth that needs to be created.

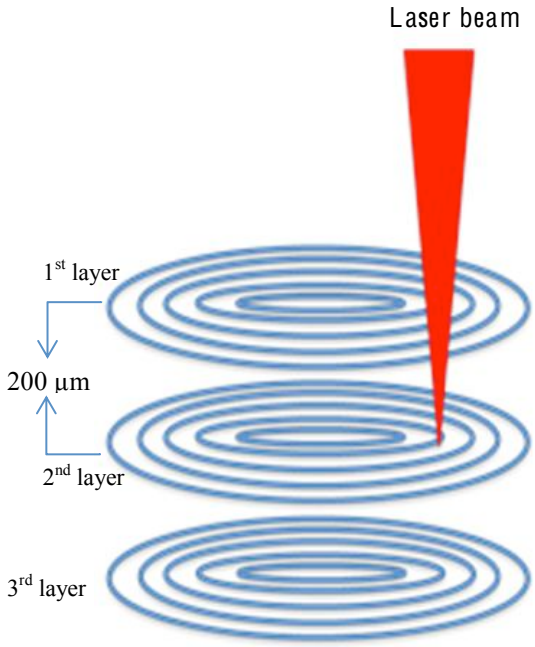

Figure 36: Concentric circles scanning procedure; 20 successive circles were ablated to create one layer, and then the beam was moved downward in the z-direction to create the second layer and so on

Thirty two holes were ablated by this strategy using different laser parameters. Some of these samples were ablated using a very low laser power of 0.64 mW with 800 μm/s scanning speed, the results showed very small depths. For example, 20 layers separated by 300 μm were created using the previous laser parameters; the measured depth was only 0.45 mm. The best ablation results were achieved by using higher laser fluences; two holes were chosen to perform the concentric scanning approach. For the first hole (Hole #1), 20 layers with 200 μm separation between the layers were scanned with 500 μm/s scanning speed, and 19.3 J/cm^2 laser fluence. Theoretically, the depth and diameter for this hole were 4 mm and 1 mm respectively, and the machining time was 28 min. The second hole (Hole #2) was created by 10 layers with 200 μm separation between the layers, using the same laser parameters. The expected depth was 2 mm which is less than the depth of the first hole. Since a lesser number of layers were used, it took less machining time (14 min).

When the ablation was done, top-view images of the two holes were taken using reflected-light microscopy. After that, the hole structures were scanned using micro-CT with x-ray tube source operating at voltage of 100 kV and 130 μA current. 3D reconstruction for the data was carried out by using Microview program.

4.2.2 Results and discussion

Top-view image of the holes were captured using reflected-light microscopy. Fig.37 a shows a microscope image of a hole scanned with 20 concentric circles. Using Northern Eclipse software, the diameter of both structures, Hole #1 and Hole #2, were measured to

be 1.09 mm and 1.03 mm respectively. The measured diameters for both holes were slightly larger than the theoretical value (1 mm) because the beam waist (~30.2 μm) was larger than the radial increment of the laser passes. Another explanation that was illustrated by Emigh is that when the pulse energy exceeds the ablation threshold, then the plasma produced by this high energy might exceed the beam waist diameter [121]. The diameter of the hole can be increased by increasing the number of concentric circles. Emigh used 40 concentric circles in his ablation in order to get 2 mm diameter hole. The image analysis that carried out by Dino Capture software showed 2.12 mm measured diameter for the hole. Fig.37 b shows a top- view image captured by digital hand-held microscope for 40 concentric circles scanned hole [121].

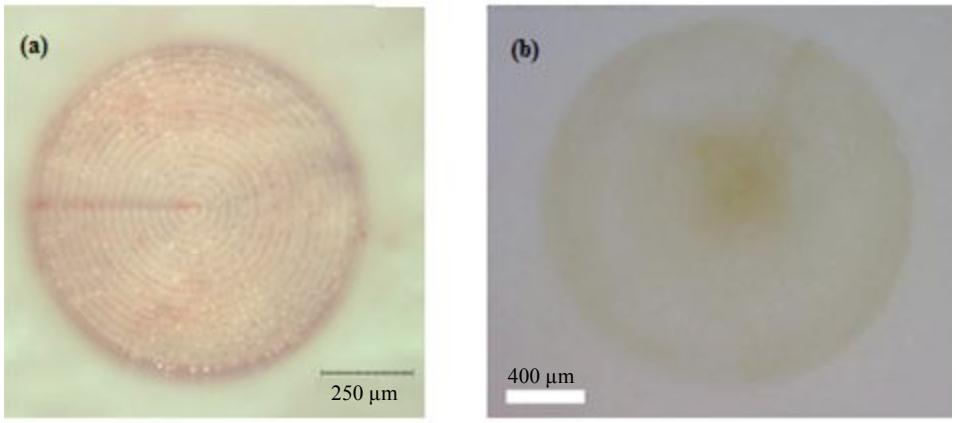

Figure 37: (a) top-view image captured by reflected-light microscopy for hole scanned with 20 concentric circles; the theoretical diameter is 1 mm (scale bar= 250 microns); (b) top-view image captured by digital hand-held microscope for hole scanned with 40 concentric circles; the theoretical diameter is 2 mm (scale bar = 400 microns). Reprinted with permission from [121]

The bone samples were scanned using micro-CT. A total of 845 projections were obtained from micro-CT scanning, which were reconstructed to 3D image with dimensions of 710 x 475 x 845 and voxel size of 0.0211 x 0.0211 x 0.0211 mm using Microview program. Fig.38 below shows micro-CT image for both hole structures, Hole #1 and Hole #2, which is reconstructed by Microview program. The walls of the ablated holes were smooth and free of damage and cracks.

Figure 38: Micro-CT image for two holes were ablated by concentric circle scanning, hole#1 has 20 layers and hole#2 has 10 layers, the successive layers were separated by 200 µm distance in both holes, (scale bar = 1 mm)

A cross section view was obtained for both hole structures, in order to measure the real depth of the holes. As shown in Fig.39. Hole #1, scanned by 20 layers with 200 µm separation between the layers, had a measured depth of 3.81 mm. Hole #2, scanned by 10 layers, had depth of 1.51 mm. The real depths for both holes were less than the expected values (4 mm for Hole #1, and 2 mm for Hole #2). This is explained by the debris that accumulates in the bottom of the hole and could not be ejected, which reduces the

ablation efficiency of the laser beam. In general, increasing the number of ablated layers or the distance between the layers may increase the depth of the hole.

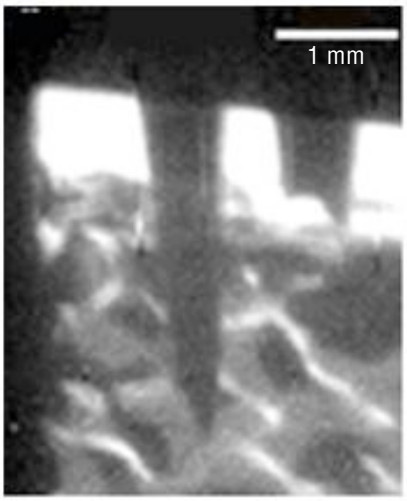

Figure 39: Micro-CT side-view image for concentric circles scanned holes, hole#1 (left) has 20 layers and hole#2 (right) has 10 layers; the successive layers were separated by 200 μm distance in both holes, (scale bar = 1 mm)

It was noticed that ablated holes have conical shapes which become more obvious with the increase in the number of layers (see Fig.39). It is thought that a decrease in ablation efficiency during drilling is responsible for this phenomenon. That can be explained by the following. When the laser beam goes deeper, the scattering of incident light increases. These scattered radiations can be absorbed by the crater walls, thereby reducing the total incident energy. A smaller region will be ablated as the laser goes deeper, leading to a smaller diameter at the bottom of the crater compared to the top, and thus creating a conical shape.

In orthopedics, bone drilling can also include the removal of trabecular bone, so the characterization of trabecular bone ablation was carried out in the previous work [121]. In that work, concentric circles were scanned on the spongy layer of scapular bone porcine samples, using 5.2 ps pulse duration, 1 kHz repetition rate, and 20.9 J/cm^2 peak fluence. A single layer of 30 concentric circles resulted in 1 mm depth and 0.5 mm diameter. Two layers separated by 200 μm were created using 30 concentric circles for each layer. This scanning resulted in 0.6 mm crater depth with 1.0 mm diameter. The crater dimensions were approximated, since the crater walls were hard to distinguish due to the diffuse nature of spongy bone. In general, the results showed that large-scale removal of trabecular bone can be achieved by concentric circles scanning. However, the trabecular cone ablation showed lower removal rate when compared to the cortical bone ablation. This was explained by the different pulse durations used in both experiments, where 170 fs was used in cortical ablation, while 2 ps was used in trabecular ablation. Another reason is that the porous nature of the spongy bone and the soft bone marrow that fills the pores increase the laser absorption during laser propagation which reduces the residual total energy of the laser [121].

A few experiments were carried out in this thesis in order to evaluate the feasibility of short pulsed lasers in trabecular bone ablation. Vertebral porcine bone was used in the ablation, where the cortical layer was removed prior the experiments. Low laser power of 41.8 mW was used with 2 ps pulse duration and 800 μm/s scanning speed, to create 20 concentric circles in two different structures. The first structure was 15 layers separated by 300 μm which resulted in 2.88 mm crater depth with 0.95 mm width. The second

structure was 20 layers separated by 200 μm, where the ablation resulted in 2.40 mm crater depth with 0.98 mm diameter. When compared to Emigh's experiment [121], these results showed larger depths, which might be due to the shorter pulse duration that was used in this experiment.

4.3 Helical scanning

4.3.1 Methods

The procedure time is an important factor to be considered in medical procedures, as it should be as short as possible. According to that, the ablation time in our previous experiments (using concentric circle scanning) was quite long, due to the ablation of the entire internal bone which is required in concentric circle scanning. In contrast, helical scanning does not require the entire bone to be removed; only the bone in the ablation path. Thus the ablation time required should be shorter when compared to the concentric circle method. This drilling strategy was previously applied on metals [147] and semiconductors [148]. In helical scanning, the beam has constant circular path diameter while the focal plane of the beam is continuously moving downward into the material, as shown in Fig.40.

The experiments were carried out on cortical bone samples that were taken from porcine vertebral bone, where three coaxial helices were ablated with diameters of 900, 950, and 1000 μm to create each hole. Each helix had 40 passes with 100 μm (Δz) vertical separation distance between successive passes.

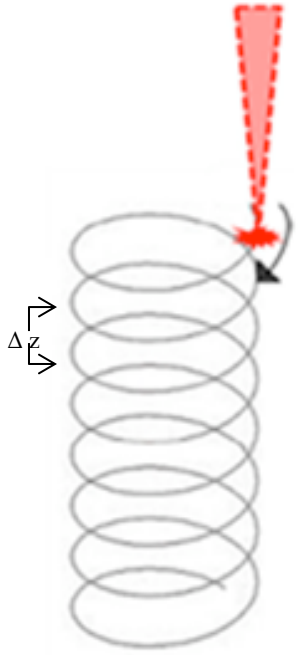

Figure 40: Helical scanning procedure, where successive passes were ablated in a helical way to create each helix. The beam was moved downward in the z-direction to a distance of Δz which is the separation distance between the successive passes

4.3.2 Results and discussion

Using this scanning strategy, a hole was created by 170 fs pulse duration, 2.6 J/cm^2 energy fluence, and 500 μm/s scanning speed laser parameters.

A reflected-light microscopy was used to capture a top-view image for the helical scanned hole, as shown in Fig.41. Northern Eclipse software, accompanied with the microscope, was used to measure the outer hole diameter, which was equal to 1.04 mm.

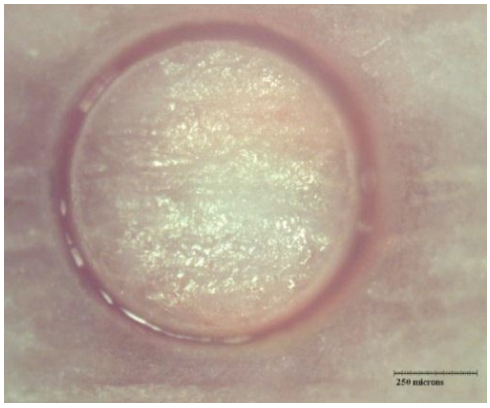

Figure 41: Top-view image captured by reflected-light microscopy for hole scanned with three coaxial helices have diameters of 900, 950, and 1000 µm, (scale bar= 250 microns)

Bone samples were scanned using micro-CT where the projections were reconstructed to 3D image, using Microview program. The image dimensions were 710 x 475 x 845 with voxel size of 0.0211 x 0.0211 x 0.0211 mm. Fig.42 a shows micro-CT image for the helical scanned hole structure.

The depth of the hole was hard to specify because of the limitation of the micro-CT resolution, however, the ablation time was less than 13 min. Fig.42 b is a side view of the 3D reconstructed micro-CT image showing the trench going through the cortical layer.

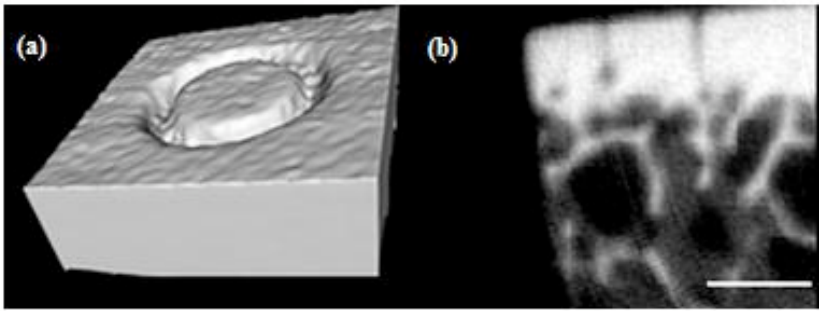

Figure 42: (a) 3D micro-CT image for a hole which was ablated by helical scanning; (b) the cross section for the ablated hole, the scale bar is 1 mm

We tried to reduce the ablation time more by reducing the number of passes. So, another hole was created after adjusting the laser fluence to 19.7 J/cm^2 and the scanning speed to 800 μm/s. Twelve passes were created with a separation of 500 μm between the successive passes. The machining time for this hole was just 2.5 minutes. However, the walls of this hole have rougher surface when compared to the previous hole which was scanned by lower laser fluence and slower scanning speed.

A micropillar always results from this scanning type (see Fig.43) which should be removed from the bone after ablation. However, if the trench reaches the trabecular bone layer, then removing the micropillar will be easier.

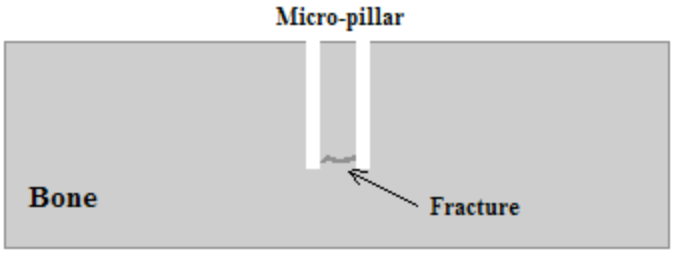

Figure 43: Micropillar that results from the helical scanning procedure; this micropillar should be removed after the ablation

It was suggested that the shock wave propagation that accompanies the plasma mediated ablation has the ability to create a fracture in the micropillar [121].

In Emigh's study, laser irradiation with 170 fs pulses, 33.4 J/cm^2 fluence, and 250 µm/s scanning speed was used to create two holes. Forty concentric circles were created in the first hole which produced a diameter of 2.12 mm and a 2.4 mm crater depth in 8.2 min machining time. For the second hole, 30 concentric circles were created in the first layer. Then the laser beam was moved downward 150 µm to create 20 concentric circles in the 2nd layer. The measured outer diameter was 1.59 mm with crater depth of 2.2 mm in a machining time of 6.5 min [121]. In our experiments, a lower laser fluence of 19.3 J/cm^2 was used when compared to the one used in the most recent work [121], in order to avoid the thermal effects and cracks. In addition, number of layers was increased to be 20 layers which led correspondingly to a longer machining time. However, our results showed greater crater depth (3.81 mm) when compared to craters that were produced in Emigh's study [121]. The long machining time problem was overcome by using helical scanning where the ablation time was reduced to 2.5 minutes only.

4.4 Effect of some laser parameters on ablation

A proper choice for laser parameters and ablation conditions leads to precise ablation with minimal collateral damage and thus an optimal ablation [73]. So, in order to increase the ablation performance, the effect of laser parameters, and most importantly the wavelength and the pulse duration on the ablation process, should be studied.

4.4.1 Effect of wavelength on bone ablation

Laser wavelength is one of the most important parameters that determine the way in which the light interacts with biological tissue (absorption, transmission, etc.). Thus a proper wavelength should be chosen for a certain application in order to get the desirable results from laser interaction [12].

However, the understanding of optical properties of the target tissue prior the ablation is the key factor in a successful choice for wavelength, which is required in a certain process. Optical properties of bone tissue, which are characterized by absorption and scattering coefficients, play a significant role in the ablation process. These properties were discussed in detail in chapter 2.

Several investigations have reported the dependence of the ablation process on laser wavelength. For example, Youn et al. investigated the ablation efficiency of a free electron laser (FEL) wavelengths, 2.79, 2.9, 6.1, and 6.45 μm. Fluence of 21.2 – 42.4 J/cm^2 with 350 ps pulse duration and 10 Hz repetition rate laser parameters were used to ablate 5x5x5 mm^3 samples of bovine knee cortical bone. The mass of removed tissue was measured using microbalance. It was found that the highest mass removed was at 6.1 μm

wavelength, which was around 5 μg/pulse, and followed by 2.9, 6.45, and 2.79 μm, respectively at all of the fluences. Laser radiation at a wavelength of 6.1 μm generated the largest crater size and the smallest thermal injury zones of less than 7 μm, however, the largest damage zone was observed at a wavelength of 2.79 μm [149].

The previous observations were explained by the optical properties effect on ablation efficiency. The 2.9 μm wavelength is strongly absorbed by water. However, applying high laser power increases tissue temperature and weakens the hydrogen bonds. This can generate thermal and mechanical transients which result in changing the optical properties of tissue, by shifting the absorption peak of water at this wavelength to shorter wavelengths. The highest ablation efficiency was at 6.1 μm where the collagen and water are important absorbers. The largest thermal damage was at 2.79 μm due to its large penetration depth into tissue [149].

Gonzalez et al. compared the thermal damage caused by CO_2 laser (10.6 μm) and Er:YAG laser (2.94 μm), in ablation of bone samples which were taken from the anterior wall of the maxillary sinuses, by applying 1 - 6 J total laser energy. The results showed that an average of 5 μm thermal damage produced by Er:YAG laser, compared to 67 μm damage with a significant char layer that was produced by CO_2 laser [150].

4.4.2 Effect of pulse duration on bone ablation

A number of studies showed that picosecond pulse ablation causes less collateral damage to the ablated tissue when compared to nanosecond duration. At picosecond pulse durations, the ablation mechanism will include non-linear absorption and multiphoton ionization processes. These processes become dominant as the pulse duration becomes shorter, until the breakdown occurs solely because of these processes for very short pulses.

In the case of ultrashort laser pulses (<10ps), as pulses become shorter, especially in femtosecond regime, the breakdown intensities become higher. At this point, just multiphoton photoionization among all the ionization processes, has the ability to produce high electron densities required for ablation. Multiphoton absorption highly depends on the intensity and that leads to a sharper ablation threshold. Another advantage for ultrashort ablation is that the laser energy is absorbed by electrons faster than being transferred to tissue. Since, the matrix is not heated during the pulse, thermal damage can occur after the pulse passes unlike at the long pulses (>50ps). While the electron density is growing, the plasma reflectivity increases and that prevent light propagation. This high density plasma has the ability to absorb 50% of the laser energy [23].

Oraevsky et al. used 1053 nm Ti: sapphire laser with pulse duration in the range of 1 ns to 350 fs to ablate collagen gel. It was found that the maximum ablation efficiency was obtained by using 350 fs pulses with fluence two times larger than the ablation threshold of the collagen gels. However, further increasing of this fluence showed a decrease in ablation depth, which was explained by the increase of plasma reflectivity [23].

The pulse duration plays a significant role in determining ablation threshold of the target material, as shorter pulses ablate at lower laser energy than the longer pulses. Giguère et al. investigated the effect of 100 fs - 5 ps pulse durations on the ablation threshold of porcine cornea, using Ti: sapphire laser of 800 nm wavelength. The results showed that the ablation threshold was almost constant in the region between 100 fs and 1 ps, and then it started increasing for longer pulses [126]. An explanation for this phenomenon was illustrated by Min Kim et al., who concluded that at long pulses, a large fraction of absorbed energy is used for tissue heating rather than tissue removal, which reduces the ablation efficiency for these pulses [131].

Chapter 5: CONCLUSION AND FUTURE WORK

Ultrashort laser ablation is considered a successful replacement for mechanical tools, since it has shown high ablation efficiency with minimal thermal damage to the surrounding tissues. In addition, other advantages that lasers have over mechanical drills include non-contact ablation, minimally invasive operation, the ability to focus at very small spots, and the absence of mechanical vibrations.

In this thesis, a review of bone histological and optical properties was completed, since bone ablation strongly depends on these properties. This leads to a better understanding of ablation mechanisms and thus the optimal parameters can be chosen for a specific ablation.

The primary parameter that should be determined prior to ablation is the ablation threshold, which is the minimum fluence required to initiate tissue removal. The ablation threshold for a material should be as low as possible to avoid excess energy deposition within the tissue so to reduce thermal damage. Researchers have attempted to reduce the ablation threshold in their studies. It was found that ultrashort laser ablation is advantageous in producing a lower ablation threshold when a higher number of incident pulses were applied, due to the incubation effect phenomenon where damage accumulation occurs.

The experiments carried out in this thesis were split into two parts. The first was the characterization of certain laser parameters and their effect on tissue ablation. The laser parameters that were investigated include pulse energy, scanning speed, number of passes, and pulse duration. Unpolished bone samples were used in order to optimize in vivo ablations.

For successful replacement of mechanical tools, laser ablation should show an ability to remove tissue on the scale of mm to cm. The second part of the experiments was to examine the feasibility of ultrashort laser in creating holes. Two different scanning strategies were used, concentric circles and helical scanning. The ablated samples were investigated by Microview program. Using the concentric circle scanning method, large ablated depths were achieved. With helical scanning, the machining time was minimized.

The repetition rate used in this study was 1 kHz, and thus the machining time could not be reduced any further. A significant reduction in the machining time can be performed when using fiber lasers with MHz repetition rates, which were recently developed.

A micro-pillar is produced after helical scanning, which must be removed to create the hole. When the trench reaches the spongy bone layer, removing the micro-pillar will be much easier; otherwise a technique to remove the micro-pillar without any side effects must be discovered.

From the experiments, it was noticed that the holes tend to have a conical shape when the number of layers increased. This can be explained by the accumulation of debris and increased beam scattering during ablation, which reduces the ablation efficiency at deeper points. A smaller exit diameter is produced compared to the entrance diameter of the hole, creating the conical shape. This conformation is undesirable in medical applications that require cylindrical holes. This issue can be a subject for future work, aiming to increase the diameter of the exit hole and trying to keep the cylindrical shape at deeper points.

Lasers can be integrated with diffuse reflectance or optical coherent tomography for real-time feedback, which adds another advantage to using lasers in orthopedics surgeries [119], and compensates for the loss of sensation that orthopedic surgeon used to have while using mechanical tools.

REFERENCES

1. Lal, H., Sharma, D., Mittal, D. (2012). Intrapelvic migration of hip lag screw of proximal femoral nail-sequele to a paradoxical reverse Z effect and their critical analysis. Journal of Clinical Orthopaedics and Trauma, 3:48–53
2. Nayak,A., Gutierrez,S., Billys,J., Santoni, B., Castellvi, A. (2013). Biomechanics of lateral plate and pedicle screw constructs in lumbar spines instrumented at two levels with laterally placed interbody cages. The Spine Journal, pii: S1529-9430(13)00400-2
3. Dental Implants. Dental implant problems (Dental Implants Corp., 2010), retrieved http://www.dental-implant-problems.com/dental-implant-procedure.html
4. Champions Innovations. Insertion procedure (Champions Innovations, 2011), retrieved www.championsinnovations.com
5. Chai, J., Hong, S., Choi, J., Koh, Y., Lee, J., Choi, J., Kang, H. (2010). Radiologic diagnosis of osteoid osteoma: from simple to challenging findings. RadioGraphics, 30:737-749
6. Atesok, K., Alman, B., Schemitsch, E., Peyser, A., Mankin, H. (2011). Osteoid osteoma and osteoblastoma. J Am Acad Orthop Surg., 19:678-89
7. Saccomanni, B. (2009). Osteoid osteoma and osteoblastoma of the spine: a review of the literature. Curr Rev Musculoskelet Med., 2: 65–67
8. The New York Times Company. Bone Tumors (The New York Times, 2013), retrieved http://health.nytimes.com/health/guides/disease/bone-tumors/
9. Bertollo, N., Walsh, W. (2011). Drilling of bone: practicality, limitations and complications associated with surgical drill-bits. ISBN 978-953-307-969-1
10. Davidson, S., James, D. (2003). Drilling in bone: modeling heat generation and temperature distribution. J Biomech Eng Trans Asme,125:305–314
11. Abukhshim, N., Mativenga, P., Sheikh, M. (2005). Investigation of heat partition in high speed turning of high strength alloy steel. International Journal of Machine Tools & Manufacture, 45:1687–1695
12. Liu, Y., Niemz, M. (2007). Ablation of femural bone with femtosecond laser pulses - a feasibility study. Lasers Med Sci, 22:171-174
13. Lo, D., Mackanos, M., Chung, M., Hyun, J., Montoro, D., Grova, M., Liu, C., Wang, J., Palanker, D., Connolly, A., Longaker, M., Contag, C., Wan, D. (2012). Femtosecond plasma mediated laser ablation has advantages over mechanical osteotomy of cranial bone. Lasers in Surgery and Medicine, 44:805–814
14. Huang, C., Liu, Y., Chen, L., Chen, Y. (2010). Temperature rise of alveolar bone during dental implant drilling using the finite element simulation. Life Science Journal, 7:68 – 72. ISSN: 1097 – 8135

15. Solon, L., Aronson, R., Gordon, G. (1961). Physiological implications of laser beams. Science, 134:1506-1508
16. Campbell, C., Noyori, K., Rittler, M., Koester, C. (1963). Intraocular temperature changes produced by laser coagulation. Acta Ophthalmol, 41:22-31
17. Kroitzsch, U., Laufer, G., Egkher, E., Wollenek, G., Horwarth, R. (1989). Experimental photoablation of meniscus cartilage by excimer laser energy: a new aspect of meniscus surgery. Arch Orthop Trauma Surg, 108:44-48
18. Schultz, R., Krishnamurthy, S., Thelmo, W., Rodriguez, J. Harvey, G. (1985). Effects of varying intensities of laser energy on articular cartilage: a preliminary study. Lasers Surg Med, 5:577-588
19. Evans, T., Winters, T., Palmeri, N., Joiner, A. (1987). Laser-assisted arthroscopic meniscal repair. South Med J., 80
20. Nuss, R., Fabian, R., Sarkar, R., Puliafito, C. (1988). Infrared laser bone ablation. Lasers Surg Med., 8:381-391
21. Niemz, M. (1996). Laser-tissue interactions: Fundamentals and applications. Springer-Verlag Berlin and Heidelberg, GmbH & Co. ISBN: 978-3-540-72191-8
22. Fork, R., Greene, I., Shank, C. (1991). Generation of optical pulses shorter than 0.1 ps by colliding pulse mode locking. Appl Phys Lett, 38:671-672
23. Oraevsky, A., Silva, L., Rubenchik, A., Feit, M., Glinsky, M., Perry, M., Mammini, B., Small, I., Stuart, B. (1996). Plasma mediated ablation of biological tissues with nanosecond-to-femtosecond laser pulses: relative role of linear and nonlinear absorption. IEEE Journal of Selected Topics in Quantum Electronics, Vol. 2
24. Newton, C., Nunamaker, D. (1985). Small Animal Orthopaedics. J.B. Lippincott Company. http://cal.vet.upenn.edu/projects/saortho/contents/contents.htm
25. Roschger, P., Misof, B., Klaushofer, K. (2012). The complexity and heterogeneity of bone material, Medicographia, 34:155-162
26. Posner, A. (1987). Bone mineral and the mineralization process. In. Bone md Mineral Research, 5: 65-116
27. Reif, J. (2010). Basic Physics of Femtosecond Laser Ablation. Springer Berlin Heidelberg, vol.130, pp 19-41. ISBN:978-3-642-03306-3
28. Ivanova, B., Hakimiana, A., Peavyb, G., Haglund Jr, R. (2003). Mid-infrared laser ablation of a hard biocomposite material: mechanistic studies of pulse duration and interface effects. Applied Surface Science, 208–209:77–84
29. Nouri, A., Hodgson, P., Wen, C. (2010). Biomimetic porous titanium scaffolds for orthopedic and dental applications. Biomimetics Learning from Nature. ISBN: 978-953-307-025-4

30. Doblaré, M. García, J., Gómez, M. (2004). Modelling bone tissue fracture and healing: a review. Engineering Fracture Mechanics, 71:1809–1840
31. Hall, S. (2006). Basic biomechanics. McGraw-Hill Humanities/Social Sciences/Languages,5 ed. ISBN-10: 0073044814
32. Clarke, B., (2008). Normal bone anatomy and physiology. Clinical Journal of the American Society of Nephrology 3. S131–S139, ISSN: 1555-9041/303–0131
33. Rho, J., Kuhn-Spearing, L., Zioupos, P. (1998). Mechanical properties and the hierarchical structure of bone. Med Eng Phys., 20:92-102
34. Khurana, J. (2009). Bone Pathology. Springer Dordrecht Heidelberg. ISBN: 978-1-58829-766-2
35. Rubin, M., Jasiuk, I., Taylor, J., Rubin, J., Ganey, T., Apkarian, R. (2003). TEM analysis of the nanostructure of normal and osteoporotic human trabecular bone. Bone, 33:270-282
36. Ivanenko, M., Werner, M., Afilal, S., Klasing, M., Hering, P. (2005). Ablation of hard bone tissue with pulsed CO_2 lasers. Medical Laser Application, 20:13-23
37. Wright, N., Humphrey, J. (2002). Denaturation of collagen via heating: an irreversible rate process. Annu. Rev. Biomed. Eng., 4:109–28
38. Vogel, A., Venugopalan, V. (2003). Mechanisms of pulsed laser ablation of biological tissues. Chem. Rev., 103:577-644
39. Forrer, M., Frenz, M., Romano, V., Altermatt, H., Weber, H., Silenok, A., Istomyn, M., Konov, V. (1993). Bone-ablation mechanism using CO_2 lasers of different pulse duration and wavelength. Appl. Phys. B, 56:104-112
40. Ivanenko, M., Hering, P. (1998). Hard tissue ablation with a mechanically Q-switched CO_2 laser, Thermal Therapy, Laser Welding and Tissue Interaction, SPIE Proc. 3565:110-115
41. Wachter, R., Stoll, P. (1991). Increase of temperature during osteotomy: in vitro and in vivo investigations. Int. J. Oral Maxillofac. Surg. 20. 245-249
42. Eriksson, R., Albrektsson, T. (1984). The effect of heat on bone regeneration: an experimental study in the rabbit using the bone growth chamber. J Oral Maxillofac Surg., 42:705-11
43. Kondo, S., Okada, Y., Iseki, H., Hori, T., Takakura, K., Kobayashi, A., Nagata, H. (2000). Thermological study of drilling bone tissue with a high-speed drill. Neurosurgery, 46:1162-8
44. Huber-Lang, M., Kovtun, A., Ignatius, A. (2013). The role of complement in trauma and fracture healing. Seminars in Immunology, 25:73– 78
45. Yacker, M., Klein, M. (1997). The effect of irrigation on osteotomy depth and bur diameter. Int J Oral Maxillofac Implants, 11:634-8

46. Oraevsky, A., Esenaliev, R., Letokhov, V. (1991). Pulsed laser ablation of biological tissue: review of the mechanisms. Lecture Notes in Physics, 389:112-122
47. Cheong, W., Prahl, S., Welch, A. (1990). A review of the optical properties of biological tissues. IEEE Journal of Quantum Electronics, 26:2166 - 2185
48. Ugnell, A., Oberg, P. (1997). The optical properties of the cochlear bone. Med. Eng. Phys., 19:630–636v
49. Youn, J., Telenkov, S., Kim, E., Bhavaraju, N., Wong, B., Valvano, J., Milner, T. (2000). Optical and thermal properties of nasal septal cartilage. Lasers in Surgery and Medicine, 27:119-128
50. Ugryumova, N., Matcher, S., Attenburrow, D. (2004). Measurement of bone mineral density via light scattering. Phys. Med. Biol., 49:469–483
51. Aoki, A., Mizutani, K., Takasaki, A., M.Sasaki, K., Nagai, S. (2008). Current status of clinical laser applications in periodontal therapy. Academy of General Density, 56:674-87
52. Tsai, C., Chen, J., Wang, W. (2001). Near-infrared absorption property of biological soft tissue constituents. Journal of Medical and Biological Engineering, 21: 7-14
53. Pal, B. (2010). Frontiers in Guided Wave Optics and Optoelectronics. INTECH, Croatia, pp. 674 ISBN 978-953-7619-82-4
54. Payne, B. (1997). The role of chromophore on pulsed laser ablation of biological tissue. Master's thesis. Retrieved from Massachusetts Institute of Technology
55. Werner, M. (2006). Ablation of hard biological tissue and osteotomy with pulsed CO_2 lasers. Doctoral thesis. Retrieved from University of Düsseldorf
56. Pirnat, S. (2007). Versatility of an 810 nm diode laser in dentistry: an overview. Journal of Laser and Health Academy Vol.2007
57. Barton, T., Foth, H., Christ, M., Hormann, K. (1997). Interaction of holmium laser radiation and cortical bone: ablation and thermal damage in a turbid medium. Optical Society of America, Applied Optics, 36:32-43
58. Steiner, R. (2011). Laser-tissue interactions. Springer Berlin Heidelberg, 23-36
59. Firbank, M., Hiraoka, M., Essenpreis, M., Delpy, D. (1993). Measurement of the optical properties of the skull in the wavelength range 650-950 nm. Phys. Med. Biol., 38:503-10
60. Chen, P., Stokes, A., McKittrick, J. (2009). Comparison of the structure and mechanical properties of bovine femur bone and antler of the North American elk (Cervus elaphus canadensis). Acta Biomaterialia, 5:693–706

61. Rossi, V., Gustafson, S., Jacques, S. (2009). Characterizing light propagation in bone for photodynamic therapy of osteosarcoma. Optics in Bone Biology and Diagnostics, 71660I SPIE Vol. 7166
62. Lange, B., Brendel, T., Hu ttmann, G. (2002). Temperature dependence of light absorption in water at holmium and thulium laser wavelengths. Optical Society of America, 41:5797-803
63. Simpson, C. (1998). Near-infrared optical properties of ex vivo human skin and subcutaneous tissues measured using the Monte Carlo inversion technique. Phys. Med. Biol., 43:2465-78
64. Heilmann, M. (2009). Laser–tissue interactions II. University of Heidelberg. retrieved http://www.umm.uni-heidelberg.de/inst/cbtm/ckm/lehre/basicoptics/6_LASER-Tissue-InteractionsII.pdf
65. Rowiak. Fundamentals of laser-tissue-interaction (Rowiak, 2013), retrieved http://www.rowiak.de/index.php?id=68
66. Linde, D., Sokolowski-Tinten, K. (2000). The physical mechanisms of short-pulse laser ablation. Applied Surface Science, 154–155:1–10
67. Albagli, D. (1994). Fundamental mechanisms of pulsed laser ablation of biological tissue. Doctoral thesis. Retrieved from Massachusetts Institute of Technology
68. Sugioka, K., Meunier, M., Alberto, A. (2010). Laser precision microfabrication. Springer Series in Materials Science. Vol. 135. ISBN 978-3-642-10523-4
69. Sarkar, R., Fabian, R., Nuss, R., Puliafito, C. (1989). Plasma-mediated excimer laser ablation of bone: a potential microsurgical tool. Am J Ololaryngol, 10:76-84
70. Welch, A., Gemert, M. (2011). Optical-thermal response of laser-irradiated tissue. Vogel, A., Venugopalan, V. Chapter 14: Pulsed Laser Ablation of Soft Biological Tissues. ISBN-10: 904818830X | ISBN-13: 978-9048188307 | Edition: 2nd ed
71. Hoffman, H., Telfair, W. (2000). Photospallation: a new theory and mechanism for mid-infrared corneal ablations. Journal of Refractive Surgery, 16: 90-94
72. Albagli, D., Dark, M., Perelman, L., Rosenberg, C., Itzkan, I., Feld, M. (1994). Photomechanical basis of laser ablation of biological tissue. Optics Letters, 19:1684-6
73. Paltauf, G., Dyer, P. (2003). Photomechanical processes and effects in ablation. Chem. Rev., 103:487-518
74. V. Venugopalan. (1995). Pulsed laser ablation of tissue: surface vaporization or thermal explosion? Laser-Tissue Interaction VI, 184 proc. SPIE2391

75. Gamaly, E., Rode, A., Tikhonchuk, V., Luther-Davies. B. (2001). Ablation of solids by femtosecond lasers: ablation mechanism and ablation thresholds for metals and dielectrics. AIP, Phys. Plasmas, 9: 949
76. Shen, N. (2003). Photodisruption in biological tissues using femtosecond laser pulses. Doctoral thesis. Retrieved from Harvard University
77. Tsai, P., Blinder, P., Migliori, B., Neev, J., Jin, Y., Squier, J., Kleinfeld, D. (2009). Plasma-mediated ablation: an optical tool for submicrometer surgery on neuronal and vascular systems. Curr Opin Biotechnol., 20: 90–99
78. Olivié, G., Giguère, D., Vidal, F., Ozaki,V., Kieffer, J., Nada, O., Brunette, I. (2008). Wavelength dependence of femtosecond laser ablation threshold of corneal stroma. Optics Express, 16:4121-4129
79. Jia, T., Chen, H., Huang, M., Zhao, F., Li, X., Xu, S., Sun, H., Feng, D., Li, C., Wang, X., Li, R., Xu, Z., He, X., Kuroda, H. (2006). Ultraviolet-infrared femtosecond laser-induced damage in fused silica and CaF_2 crystals. Physical Review B, 73:1-9
80. Prasad, P. (2003). Introduction to Biophotonics. Wiley-Interscience, ed.1. ISBN 0-471-28770-9
81. Darbar, A., Darbar, R. (2010). Introduction to laser dentistry: part one. Aesthetic Dentistry Today, 4:17-21
82. Henn, K., Gubaidullin, G., Bongartz, J., Wahrburg, J., Roth, H., Kunkel, M. (2013). A spectroscopic approach to monitor the cut processing in pulsed laser osteotomy. Lasers Med Sci., 28:87–92
83. Berlien H., Krasner, N., Okunata,T., Sliney, D., Berlien, H., Müller, G. (2003). Applied laser medicine. Springer, ed.1. ISBN: 978-3-642-62391-2
84. Dressel, M., Jahn, R., Neu, W., et al. (1991). Studies in fiber guided excimer laser surgery for cutting and drilling bone and meniscus. Lasers Surg. Med., 11:569–579
85. Yow, L., Nelson, J.S., and Berns, M.W. (1989). Ablation of bone and polymethylmethacrylate by an XeCl (308-nm) excimer laser. Lasers Surg. Med., 9:141–147
86. Obara, T., Munin, E., Libert, E., Pompeu, E., Pacheco, M. (2005). XeCl excimer laser ablation of rabbit tibia bone: morphology of the irradiated site and self-limiting effect. Photomedicine and Laser Surgery, 23:561-6
87. König, H., Bücker, G., Stefanec, A., et al. (1993). Photoablation via excimer laser beam—a suitable concept for microneurosurgery? Neurochirurgia, 36:105–109
88. Walter, M., Domes, M., Diller, R., et al. (1999). Photoablation of bone by excimer laser radiation. Lasers Surg. Med., 25:153–158

89. Paschotta, R. CO_2 Lasers. RP Photonics Encyclopedia, retrieved http://www.rp-photonics.com/CO_2_lasers.html
90. Walsh, J. (1988). Pulsed laser ablation of tissue: analysis of the removal process and tissue healing. Doctoral thesis. Retrieved from Massachusetts Institute of Technology
91. George, R., Walsh, L. (2007). Coaxial water mist spray alters the ablation properties of human radicular dentine for the holmium: YAG laser. J Oral Laser Applications, 7:225-231
92. Frentzen M, Gotz W, Ivanenko M, Afilal S, Werner M, Hering P. (2003). Osteotomy with 80-ms CO_2 laser pulses—histological results. Lasers Med Sci, 18:119–124
93. Fan, K., Bell, P., Fried, D. (2006). Rapid and conservative ablation and modification of enamel, dentin, and alveolar bone using a high repetition rate transverse excited atmospheric pressure CO_2 laser operating at λ=9.3μm. J. Biomed. Opt., 11:1-11
94. Perez, M., Bank, D. (1998). Facial skin resurfacing with the erbium: YAG laser: new findings. Cosmetic Dermatology, 11:27-37
95. Bader, C., Dent, M., Krejci, I. (2006). Indications and limitations of Er: YAG laser applications in dentistry (review article). Am J Dent, 19:178-186
96. Ishikawa, I., Aoki, A., Takasaki, A. (2008). Clinical application of erbium: YAG laser in periodontology. J Int Acad Periodontol, 10:22-30
97. Hohenleutner, U., Hohenleutner, S., Baumler, W., Landthaler, M. (1997). Fast and effective tissue ablation rates and thermal damage zones. Laser Surg Med. 20:242-247
98. Sasaki, K., Aoki, A., Masuno, H., Ichinose, S., Yamada, S., Ishikawa, I. (2002). Compositional analysis of root cementum and dentin after Er:YAG laser irradiation compared with CO_2 laser and intact roots. Journal of Periodontal Research. ISSN 0022-3484
99. Gaspirc, B., Skaleric, U. (2001). Morphology, chemical structure and diffusion processes of root surface after Er:YAG and Nd:YAG laser irradiation. J Clin Periodontol, 28:508–516
100. Armengol, V., Jean, A., Marion D. (2000). Temperature rise during Er:YAG and Nd:YAP laser ablation of dentin. Journal of Engowntics, 26:138-41
101. Trimedyne. Medical Information (Trimedyne, Inc. 2002), retrieved http://www.trimedyne.com/education.htm
102. Kabalin, J., Gilling, P., Fraundorfer, M. (1998). Application of the holmium: YAG laser for prostatectomy. J Clin Laser Med Surg., 16:21-7

103. Chepurov, A., Nemenova, A., Mazo, E. (1996). Methods of fragmentation of ureteral stones using the Ho-YAG-laser. European Urology, 30:125
104. Chang, Y., Chen, C. (2000). Application of the holmium: YAG laser for ureteral and urethral disease: experience in minimally invasive endourology in chang gung memorial hospital. J Urol R.O.C., 11:51-55
105. Johnson, D. (1994). Use of the holmium: YAG (Ho:YAG) laser for treatment of superficial bladder carcinoma. Lasers in Surgery and Medicine, 14:213-218
106. Hafez, M., Coombs, R., Zhou, S., McCarthy, I. (2000). Ablation of bone, cartilage, and facet joint capsule using Ho:YAG laser. J Clin Laser Med Surg., 20:251-5
107. Charlton, A., Dickinson, M., King, T., Freemont, A. (1990). Erbium-YAG and holmium-YAG laser ablation of bone. Lasers in Medical Science, 5:365-373
108. Chanthaboury, R., Irinakis, T. (2005). The use of lasers for periodontal debridement: marketing tool or proven therapy? Dip Perio., 71:653-658
109. Green, J., Kaufman, J. (2012). Long-pulsed 1,064 nm Nd:YAG lasers effective in vein, PWS, other treatments. Dermatology Times. http://dermatologytimes.modernmedicine.com/dermatology-times/news/modernmedicine/modern-medicine-now/long-pulsed-1064-nm-ndyag-lasers-effective
110. Weiss, R., Weiss M. (1999). Early clinical results with a multiple synchronized pulse 1064 nm laser for leg telangiectasias and reticular veins. Dermatol Surg, 25:399-402
111. http://orthopedics.about.com/cs/arthroscopy/a/arthroscopy.html
112. Siebert, W. (2001). History of lasers in orthopedic medicine. Springer Berlin Heidelberg, pp 3-6. ISBN:978-3-642-56420-8
113. O'Brien, S., Fealy, S., Gibney, M., Miller, D., Kelly, A. (1990). Arthroscopic contact Nd: YAG laser meniscectomy: basic science, surgical technique, and clinical follow up. Proc. SPIE 1200, Laser Surgery: Advanced Characterization, Therapeutics, and Systems II, 224
114. Atik, O., Sener, E., Bölükbasi, E., Cila, E. (1993). Nd:YAG contact laser arthroscopy: preliminary report. Journal of Islamic Academy of Sciences, 6:131-132
115. Rybak, L., Gangi, A., Buy, X., Vieira, R., Wittig, J. (2010). Thermal ablation of spinal osteoid osteomas close to neural elements: technical considerations. AJR Am. J. Roentgenol, 195:W293-8
116. Hipdysplasia. Osteotomy (International Hip Dysplasia Institute, 2012), retrieved http://www.hipdysplasia.org/developmental-dysplasia-of-the-hip/child-treatment-methods/osteotomy/

117. WebMD. Osteotomy for Osteoarthritis (WebMD, 2005), retrieved http://www.webmd.com/osteoarthritis/osteotomy-for-osteoarthritis
118. Papadaki, M., Doukas, A., Farinelli, W., Kaban, L., Troulis, M. (2007). Vertical ramus osteotomy with Er:YAG laser: a feasibility study. Int. J. Oral Maxillofac. Surg. 36:1193–1197
119. An, R., Khader, G., Wilk, E., Emigh, B., Haugen, H., Wohl, G., Dunlop, B., Anvari, M., Fang. Q. (2013). Ultrafast laser ablation and machining large size structures on porcine bone. J. Biomed. Opt., 18, 070504
120. Newport. Gaussian Beam Optics, retrieved http://www.rpgroup.caltech.edu/courses/aph162/2007/Protocols/Optics/e3872_Gaussian-Beam-Optics.pdf
121. Emigh, B. (2011). Experimental Evaluation of Bone Drilling using Ultrashort Pulsed Laser Ablation. Master's thesis. Retrieved from McMaster University
122. Devlin H., Dickinson, M., Freemont, A., King, T., Lloyd, R. (1994). Healing of bone defects prepared using the erbium-YAG laser. Laser Med Sci, 9:239-242
123. Farley, J., Hall, S., Ilacas, D., Orcutt, C., Miller, B., Hill, C., Baylink, D. (1994). Quantification of skeletal alkaline-phosphatase in osteoporotic serum by wheat-germ-agglutinin precipitation, heat inactiviation, and a 2-site immunoradiometric assay. Clin Chem, 40:1749-1756
124. Armstrong, W., Neev, J., Da Silva, L., Rubenchik, A., Stuart, B. (2002). Ultrashort pulse laser ossicular ablation and stapedotomy in cadaveric bone. Laser Surg Med, 30:216-220
125. Ben-Yakar A., Byer, R. (2004). Femtosecond laser ablation properties of borosilicate glass. J Appl. Phys., 96:5316-5323
126. Giguère, D., Olivié, G., Vidal, F., Toetsch, S., Girard, G., Ozaki, T., Kieffer, J., Nada, O., Brunette, I. (2007). Laser ablation threshold dependence on pulse duration for fused silica and corneal tissues: experiments and modeling. JOSA A, 24:1562-1568
127. Sanner , N., Utéza, O., Bussiere, B., Coustillier, G., Leray, A., Itina, T., Sentis, M. (2009). Measurement of femtosecond laser-induced damage and ablation thresholds in dielectrics. Appl. Phys., 94:889–897
128. Kang, H., Oh, J., Welch, A. (2008). Investigations on laser hard tissue ablation under various environments. Phys. Med. Biol., 53:3381-3390
129. Girard, B., Yu, D., Armstrong, M., Wilson, B., Clokie, C., Miller, R. (2007). Effects of femtosecond laser irradiation on osseous tissues. Laser Surg. Med., 39:273-285
130. Serbin, J., Bauer, T., Fallnich, C., Kasenbacher, A., Arnold, W. (2002). Femtosecond lasers as novel tools in dental surgery. Appl. Surf. Sci., 197:737-740

131. Kim, B., Feit, M., Rubenchik, A., Joslin, E., Celliers, P., Eichler, J., Da Silva, L. (2001). Influence of pulse duration on ultrashort laser pulse ablation of biological tissues. J Biomed Opt, 6:332-338
132. Stuart, B., Feit, M., Herman, S., Rubenchik, A., Shore, B., Perry, M. (1996). Nanosecond to femtosecond laser-induced breakdown in dielectrics. Phys. Rev. B (Condensed Matter), 53:1749-1761
133. Stern, D., Schoenlein, R., Puliafito, C., Dobi, E., Birngruber, R., Fujimoto, J. (1989). Corneal ablation by nanosecond, picosecond, and femtosecond lasers at 532 and 625 nm. Arch Ophthalmol, 107:587-92
134. Murray, A., Dickinson, M. (2004). Tissue ablation-rate measurements with a long-pulsed, fibre-deliverable 308 nm excimer laser. Lasers in Medical Science, 19:127–138
135. Loesel, F., Niemz, M., Bille, J., Juhasz, T. (1996). Laser-induced optical breakdown on hard and soft tissues and its dependence on the pulse duration: experiment and model. IEEE Journal of Quantum Electronics, 32: 1717-1722
136. Emigh, B., An, R., Hsu, E., Crawford, T., Haugen, H., Wohl, G., Hayward, J., Fang, Q. (2012). Porcine cortical bone ablation by ultrashort pulsed laser irradiation. Journal of Biomedical Optics, 17:1-6
137. Nielsen, J. (2010). Short-pulse laser ablation of metals: fundamentals and applications for micro-mechanical interlocking. Doctoral thesis. Retrieved from University of Aarhus
138. Lim, Y., Altman, K., Farson, D., Flores, K. (2009). Micropillar fabrication on bovine cortical bone by direct-write femtosecond laser ablation. J Biomed Opt, 14:1-10
139. Kim, B., Feit, M., Rubenchik, A., Joslin, E. (2000). Effects of high repetition rate and beam size on hard tissue damage due to subpicosecond laser pulses. Applied Physics Letters, 76:4001 - 4003
140. Borowiec, A., Haugen, H. (2004). Femtosecond laser micromachining of grooves in indium phosphide. Appl. Phys. A., 79:521–529
141. Obara, M., Ozono, K., Kanai, M., Sekita, H., Atanasov, P. (2003). Femtosecond laser processing tailored for biomedical materials and laser power delivery through optical fibers. Proc. SPIE 4977. Photon Processing in Microelectronics and Photonics II, 123
142. Johar, K. (2011). Fundamentals of laser dentistry. JP Medical Ltd. ISBN-10: 9350253771
143. Qiu, J., Joel, M., Teichman, H., Wang, T., Neev, J., Glickman, R., Chan, K., Milner, T. (2010). Femtosecond laser lithotripsy: feasibility and ablation mechanism. Journal of Biomedical Optics 15:1-5

144. Erkan, S., Hsu, B., Wu, C., Mehbod, A., Perl, J., Transfeldt, E. (2010). Alignment of pedicle screws with pilot holes: can tapping improve screw trajectory in thoracic spines? Eur Spine J, 19:71-77
145. Jacofsky, D., Frassica, D., Frassica, F. (2004). Metastatic disease to bone. Hospital Physician, 39:21-28
146. IAEA. (2007). Criteria for Palliation of Bone Metastases – Clinical Applications. -TECDOC-1549. ISBN:92-0-104507-7
147. Michalowski, A., Walter, D., Dausinger, F., Graf, T. (2008). Melt dynamics and hole formation during drilling with ultrashort pulses. J Laser Micro/Nanoengineering, 3:211-215
148. Kaspar, J., Luft, A., Nolte, S., Will, M., Beyer, E. (2006). Laser helical drilling of silicon wafers with ns to fs pulses: Scanning electron microscopy and transmission electron microscopy characterization of drilled through-holes. J. Laser Appl. 18:85-92
149. Youn, j., Sweet, P., Peavy, G. (2007). A comparison of mass removal, thermal injury, and crater morphology of cortical bone ablation using wavelengths 2.79, 2.9, 6.1, and 6.45 μm. Lasers in Surgery and Medicine, 39:332–340
150. Gonzalez, C., Merwe, W., Smith, M., Reinisch, L. (1990). Comparison of the erbium-yttrium aluminum garnet and carbon dioxide lasers for in vitro bone and cartilage ablation. Laryngoscope, 100:14-7